Since January 2020 Elsevier has created a COVID-19 resource centre with free information in English and Mandarin on the novel coronavirus COVID-19. The COVID-19 resource centre is hosted on Elsevier Connect, the company's public news and information website.

European Journal of Medicinal Chemistry 257 (2023) 115487

Contents lists available at ScienceDirect

European Journal of Medicinal Chemistry

journal homepage: www.elsevier.com/locate/ejmech

Research paper

Discovery of quinazolin-4-one-based non-covalent inhibitors targeting the severe acute respiratory syndrome coronavirus 2 main protease (SARS-CoV-2 M^{pro})

Kuojun Zhang [a,1], Tianyu Wang [a,1], Maotian Li [c,1], Mu Liu [d], He Tang [a], Lin Wang [a], Ke Ye [a], Jiamei Yang [a], Sheng Jiang [a], Yibei Xiao [a], Youhua Xie [d,***], Meiling Lu [c,**], Xiangyu Zhang [b,*]

[a] Department of Medicinal Chemistry, School of Pharmacy, China Pharmaceutical University, Nanjing, 210009, China
[b] Department of Biomedical Engineering, School of Engineering, China Pharmaceutical University, Nanjing, 210009, China
[c] Department of Pharmacology, School of Life Science and Technology, China Pharmaceutical University, Nanjing, 210009, China
[d] Key Laboratory of Medical Molecular Virology (MOE/NHC/CAMS), Shanghai Institute of Infectious Diseases and Biosecurity, School of Basic Medical Sciences, Fudan University, 200032, Shanghai, China

ARTICLE INFO

Handling Editor: Dr. Z Liu

Keywords:
SARS-CoV-2 M^{pro}
Noncovalent M^{pro} inhibitors
Antiviral drugs
Antiviral activity

ABSTRACT

The COVID-19 pandemic caused by SARS-CoV-2 continues to pose a great threat to public health while various vaccines are available worldwide. Main protease (M^{pro}) has been validated as an effective anti-COVID-19 drug target. Using medicinal chemistry and rational drug design strategies, we identified a quinazolin-4-one series of nonpeptidic, noncovalent SARS-CoV-2 M^{pro} inhibitors based on baicalein, 5,6,7-trihydroxy-2-phenyl-4*H*-chromen-4-one. In particular, compound **C7** exhibits superior inhibitory activity against SARS-CoV-2 M^{pro} relative to baicalein (IC_{50} = 0.085 ± 0.006 and 0.966 ± 0.065 μM, respectively), as well as improved physicochemical and drug metabolism and pharmacokinetics (DMPK) properties. In addition, **C7** inhibits viral replication in SARS-CoV-2-infected Vero E6 cells more effectively than baicalein (EC_{50} = 1.10 ± 0.12 and 5.15 ± 1.64 μM, respectively) with low cytotoxicity (CC_{50} > 50 μM). An X-ray co-crystal structure reveals a non-covalent mechanism of action, and a noncanonical binding mode not observed by baicalein. These results suggest that **C7** represents a promising lead for development of more effective SARS-CoV-2 M^{pro} inhibitors and anti-COVID-19 drugs.

1. Introduction

The Coronavirus Disease 2019 (COVID-19) pandemic caused by severe acute respiratory syndrome coronavirus 2 (SARS-CoV-2) has heavily impacted the global economy and threatened public health. According to the World Health Organization (WHO) report, there have been more than 645 million confirmed cases of COVID-19 worldwide, including more than 6.6 million deaths, as of 13 December 2022 [1]. Since the outbreak of COVID-19, enormous global efforts from academic and pharmaceutical companies have been made to discover preventive and therapeutic strategies to fight against this life-threatening disease [2,3]. To date, more than 20 effective SARS-CoV-2 vaccines have been made available globally, and play an important preventive role in controlling the COVID-19 pandemic. Nevertheless, a large number of people have not yet been vaccinated due to personal unwillingness or limited medicinal conditions; on the other hand, increasing numbers of breakthrough infections have been observed in convalescent and/or vaccinated populations, mainly due to decline in protective efficacy of vaccines with time since vaccination, or compromised effectiveness against the emerging omicron variants and subvariants [4–8]. Accordingly, the public are still at high risk of being infected, and effective antiviral drugs against SARS-CoV-2 and its emerging variants are still highly needed.

A large number of anti-COVID-19 drug targets have been reported,

* Corresponding author.
** Corresponding author.
*** Corresponding author.
E-mail addresses: yhxie@fudan.edu.cn (Y. Xie), lumeiling@cpu.edu.cn (M. Lu), xiangyu.zhang@cpu.edu.cn (X. Zhang).
[1] Kuojun Zhang, Tianyu Wang and Maotian Li contributed equally to this work.

https://doi.org/10.1016/j.ejmech.2023.115487
Received 28 February 2023; Received in revised form 30 April 2023; Accepted 13 May 2023
Available online 24 May 2023

with SARS-CoV-2 main protease [M^{pro}; also known as 3C-like (3CL) protease or nonstructural protein 5 (nsp5)] capturing much attention. M^{pro} has been validated as an effective target for development of orally available small-molecule antiviral drugs [9,10]. M^{pro} cleaves viral polyproteins at 11 distinct sites to release functional non-structural proteins (nsps) that are essential for viral replication. Inhibition of M^{pro} is therefore able to block the viral replication and shut down the viral life cycle. Moreover, M^{pro} features a unique substrate specificity of glutamine (Gln) at the P1 position and no homologous human proteases have been known, and hence M^{pro} inhibitors are likely to cause no side-effects by interfering with host proteases. In contrast, M^{pro} are highly conserved among various coronaviruses, such as SARS-CoV-2, SARS-CoV and

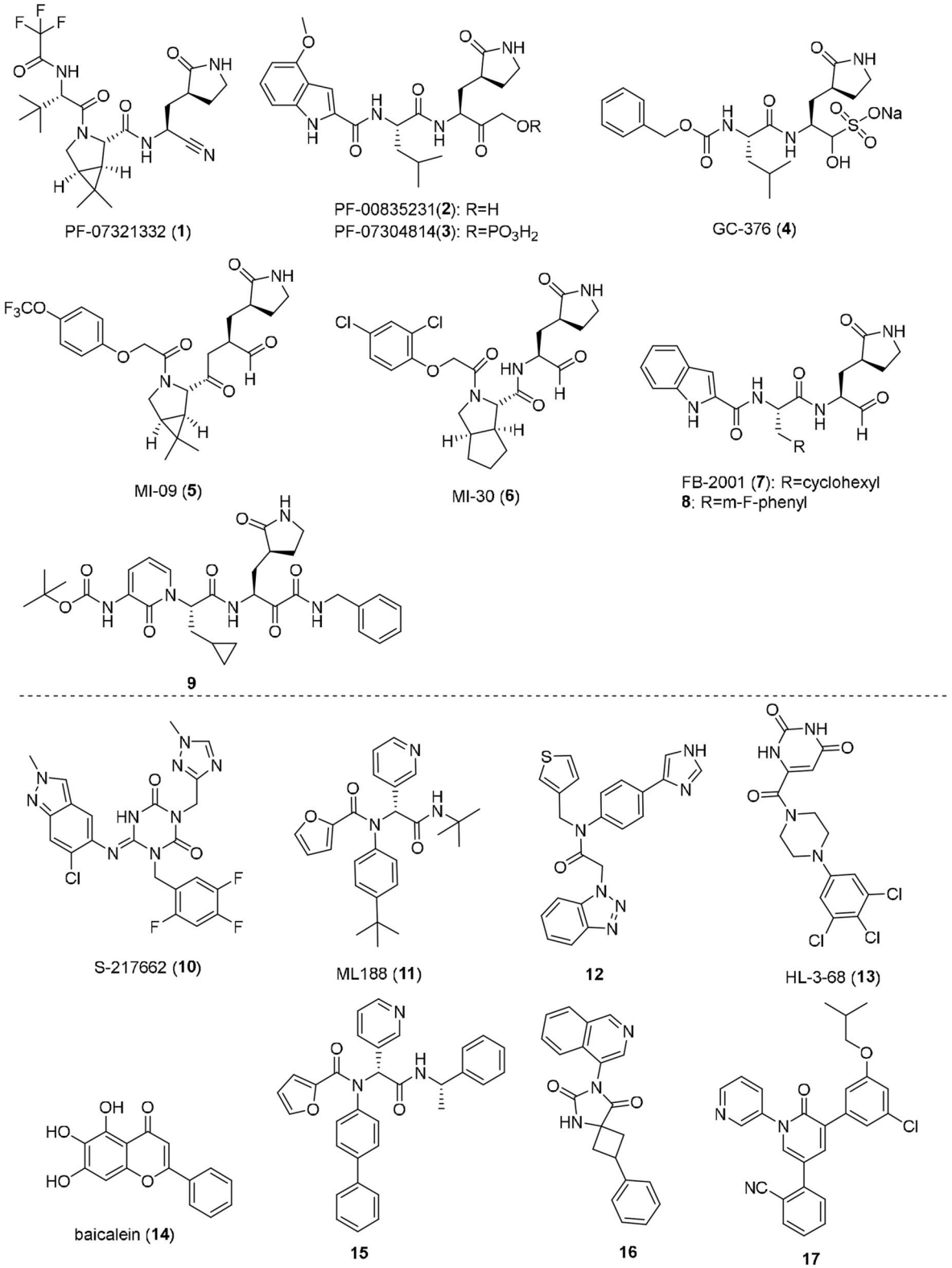

Fig. 1. Chemical structures of representative peptide-like covalent, and nonpeptidic, noncovalent SARS-CoV-2 M^{pro} inhibitors.

MERS, making it a promising target for development of broad-spectrum coronavirus antivirals. Notably, M^{pro} inhibitors should be effective against all the emerging variants of SARS-CoV-2, since the mutations occurring in spike proteins of variant strains cannot affect M^{pro}, and M^{pro} itself was shown to have an extremely low mutation rate in the emerging SARS-CoV-2 variants [10–12]. To date, a large number of SARS-CoV-2 M^{pro} inhibitors have been reported, and are mainly divided into two types: peptide-like covalent inhibitors represented by nirmatrelvir (PF-07321332, **1**) [13], PF-00835231 (**2**) [14], PF-07304814 (**3**) [15], GC-376 (**4**) [16], MI-09 (**5**), MI-30 (**6**) [17] and compounds (**7**–**9**) [18,19], as well as nonpeptidic, noncovalent inhibitors represented by Ensitrelvir (S-217622, **10**) [11], ML-188 (**11**), compound **12** [20], HL-3-68 (**13**) [21], baicalein (**14**) [22] and compounds **15**–**17** [23–25] (Fig. 1). Potential off-target effects, low membrane permeability and poor metabolic stability pose challenges for the extensive clinical application of peptidelike covalent inhibitors, notwithstanding the approval of Paxlovid (a combination of PF-07321332 and ritonavir) by the US Food and Drug Administration (FDA). The nonpeptidic, non-covalent M^{pro} inhibitor seems to be a more attractive modality. Ensitrelvir (S-217622) developed by Shionogi & Co., Ltd. showed robust antiviral potency against SARS-CoV-2 and its variants, excellent selectivity for M^{pro} over host proteases, as well as an outstanding DMPK profile in preclinical models [11]. Ensitrelvir (S-217622) exhibited promising single-agent antiviral potency and safety profiles in phase II/III clinical trials [26]. More recently, it was approved for clinical application by the Pharmaceuticals and Medical Device Agency (PMDA). But effective nonpeptidic, non-covalent M^{pro} inhibitors are very limited, and it is still necessary to search for more non-covalent M^{pro} inhibitors with diverse chemical scaffolds and improved properties.

Here, we describe our discovery of quinazolin-4-one-based nonpeptidic, non-covalent inhibitors of SARS-CoV-2 M^{pro} that are derived from baicalein (**14**). Baicalein was the first reported nonpeptidic, non-covalent inhibitor of SARS-CoV-2 M^{pro} discovered by Shanghai Institute of Materia Medica, Chinese Academy of Sciences [22], and its good biochemical and cellular antiviral activity captured our interest. Nevertheless, the potency of baicalein requires further structural optimization and extensive structure activity relationship (SAR) studies. Moreover, the drug metabolism and pharmacokinetics (DMPK) properties and target specificity were largely unknown. In order to fill in gaps in this area and explore the potential of this series as a lead for the development of anti-COVID-19 drugs, we firstly used a scaffold hopping strategy turning baicalein's chromen-4-one core to the alternative privileged scaffold, quinazolin-4-one. In this way, we discovered the first quinazolin-4-one-based SARS-CoV-2 M^{pro} inhibitor, and further structural optimizations allowed us to produce quinazolin-4-one-based SARS-CoV-2 M^{pro} inhibitors that are superior to baicalein in terms of biochemical potency, cellular antiviral activity and DMPK profile. An X-ray cocrystal structure of **D8** in SARS-CoV-2 M^{pro} revealed a ligand-induced conformation change, which allows the *sec*-butyl moiety of **D8** to occupy a newly formed binding site between the canonical S1′ and S2 subpockets, suggesting a binding mode to M^{pro} of quinazolin-4-one-based SARS-CoV-2 M^{pro} inhibitors that is different from that of baicalein.

2. Results and discussion

2.1. Design of the quinazolin-4-one class of SARS-CoV-2 M^{pro} inhibitors

The active site of M^{pro} is composed of five subpockets, S4–S1′, which can accommodate substrate and inhibitor groups at positions P4–P1′, with a Cys145-His41 catalytic dyad. As summarized by researchers from Shionogi Pharmaceutical in a recent publication, the pharmacophore based on the known M^{pro} inhibitors generally includes: (i) a hydrogen acceptor that interacts with the side-chain NH of His163 in the S1 subpocket, (ii) a hydrogen acceptor that forms a hydrogen bond with the main-chain NH of Glu166, and (iii) a lipophilic group in the S2 subpocket [11]. As shown in Fig. 2A, the cocrystal structure of baicalein (**14**) in SARS-CoV-2 M^{pro} (PDB code: 6M2N [22]) showed that baicalein follows this pharmacophore model. Specially, three phenolic hydroxyl groups in baicalein form a hydrogen-bond network with the side chains of Ser144/His163 and main chains of Leu141/Gly143 directly or indirectly through water molecules. The carbonyl group at C4 position forms a critical hydrogen bond with the Glu166. Accordingly, three phenolic hydroxyl groups and C4 carbonyl group are necessary for the potency, and therefore were retained in our design. The free phenyl ring (C ring) occupies the S2 subpocket with extensive hydrophobic interactions. The core chromen-4-one forms many key interactions contributing to baicalein's binding affinity with protein: (i) the A ring forming *S*–π and NH_2–π with the catalytic Cys145 and Asn142, respectively; (ii) the B ring π–π stacking with catalytic His41, and forming hydrophobic interactions with Met165. In addition, the chromen-4-one motif acts as a scaffold to assemble these necessary components. We envisioned that other aromatic heterocycles with similar structure could replace the chromen-4-one structure in baicalein. Because quinazolin-4-one and quinolin-4-one have been often seen in many natural products, biologically active compounds and clinically used drugs, together with well-established efficient synthesis and functionalization methodologies of these heterocycles, we firstly used a scaffold hopping strategy to replace the core chromen-4-one in baicalein with quinazolin-4-one or quinolin-4-one, respectively, in order to discover structurally novel non-covalent M^{pro} inhibitors. The resulting quinolin-4-one-based compound **18** had a complete loss of M^{pro} enzymatic inhibitory activity, while quinazolin-4-one-based compound **19** exhibited comparable inhibitory activity with that of baicalein. Therefore, we proceeded with **19** as a lead compound. A step-by-step optimization strategy and SAR studies of substituent groups at the C2 and N3 positions of quinazolin-4-one were conducted (Fig. 2B). Finally, the optimal substituents at the C2 and N3 positions were integrated, leading to a series of potent SARS-CoV-2 M^{pro} inhibitors (Fig. 2B).

2.2. Chemistry

As shown in Scheme 1, the quinolin-4-one derivative **18** was obtained by the base-mediated cyclization of *N*-(ketoaryl)amide (the Camps cyclization) according to the published literature [27]. Condensation of compound **20** and benzoyl chloride afforded benzamide (**21**). The Friedel-Crafts acylation of **21** using acetyl chloride in the presence of $SnCl_4$ gave the cyclization precursor (**22**) [28], which was then cyclized at 110 °C in the presence of KOH to generate compound **23** [27], and this was followed by BBr_3-mediated demethylation to yield the desired product (**18**).

There are many efficient ways to construct quinazolin-4-one derivatives. We selected the appropriate synthetic method for each target compound based on the availability of raw materials. Compounds **A1**–**A6**, **A8**–**A12**, **A14**, **A16**, **A18**, **A19**, **A21**–**A27** and **19** were obtained in two steps: (i) the reaction of key intermediate **24** [29] with various amidine hydrochlorides **25a**–**25w** that are commercially available or easily synthesized in efficient mild copper-catalyzed conditions to yield compounds **26a**–**26w** [30]; (ii) BBr_3-mediated demethylation of compounds **26a**–**26w** (Scheme 2). A one-pot I_2-mediated oxidative cyclization of *o*-anthranilamide **27** [31] and various commercially available aldehydes **28a**–**28v** [32] and subsequent demethylation were used to synthesize compounds **A7**, **A13**, **A15**, **A17**, **A20** and compounds **B1**–**B17** (Scheme 3). As depicted in Scheme 4, the N_3 substituted quinazolin-4-one derivatives **C1**–**C15** were prepared by condensation of the prepared *o*-anthranilamides **30a**–**30o** with benzaldehyde under similar reaction conditions with B series compounds followed by demethylation. Compounds **D6**–**D9** were obtained by the oxidative cyclization approach that was used to access compounds in the B and C series in a good yield (Scheme 7), but compounds **D1**–**D5** and **D10**–**D12** could not be synthesized under the same conditions. **D1**–**D4**, **D10** and **D11** were successfully achieved by cyclization of *N*-acylanthranilic acids

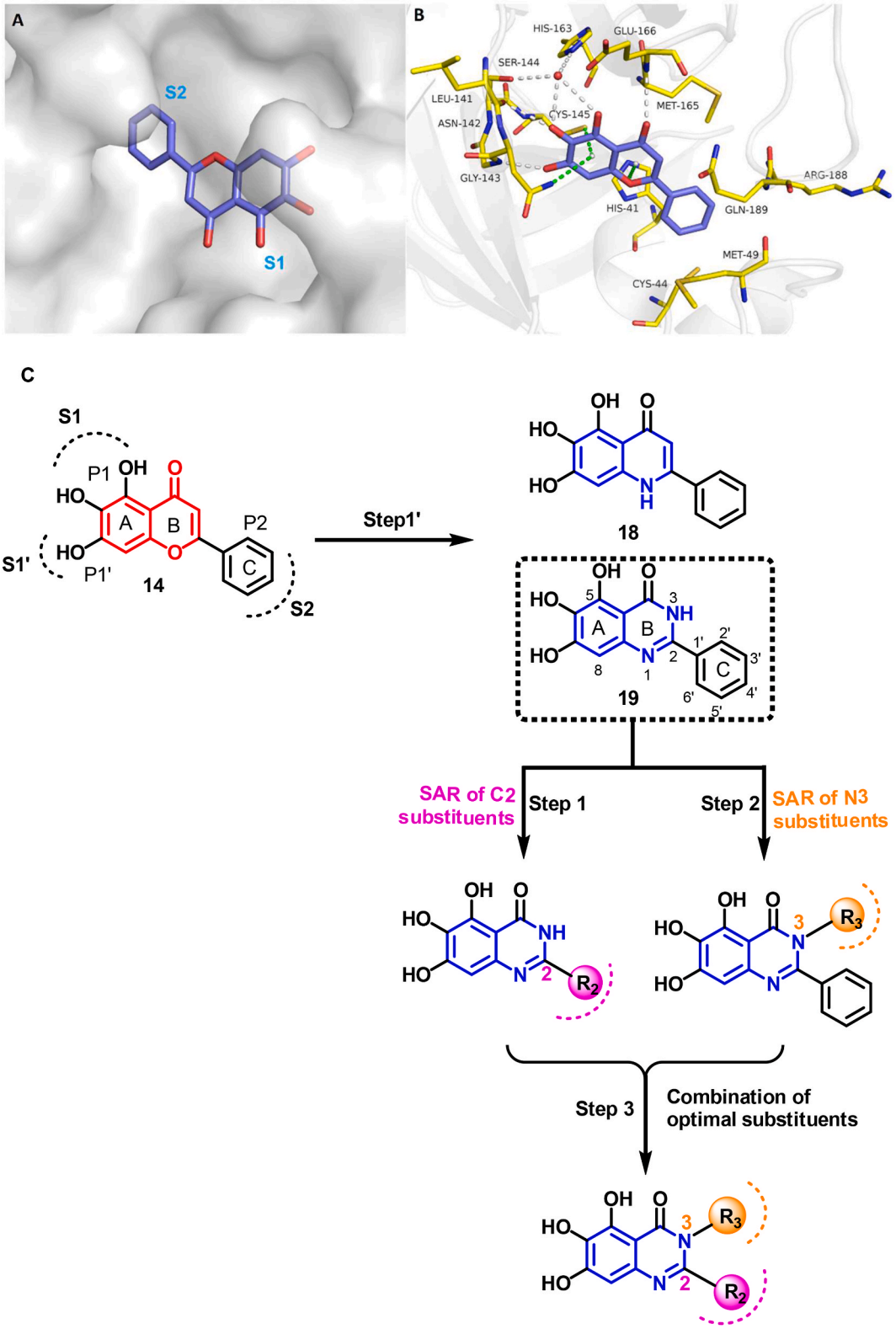

Fig. 2. Rational design of non-covalent SARS-CoV-2 M^{pro} inhibitors. (A) Binding pocket of baicalein in SARS-CoV-2 M^{pro} (PDB code 6M2N). (B) Detailed binding mode of baicalein complexed with M^{pro}. The protein is shown in gray cartoon, baicalein in blue sticks, and the selected residues in yellow sticks. Hydrogen bonds are indicated as gray dashes, and water molecule as red sphere. S–π, NH_2–π and π–π stacks are indicated as green dashes. (C) Step-by-step optimization strategy of non-covalent SARS-CoV-2 M^{pro} inhibitors starting from baicalein.

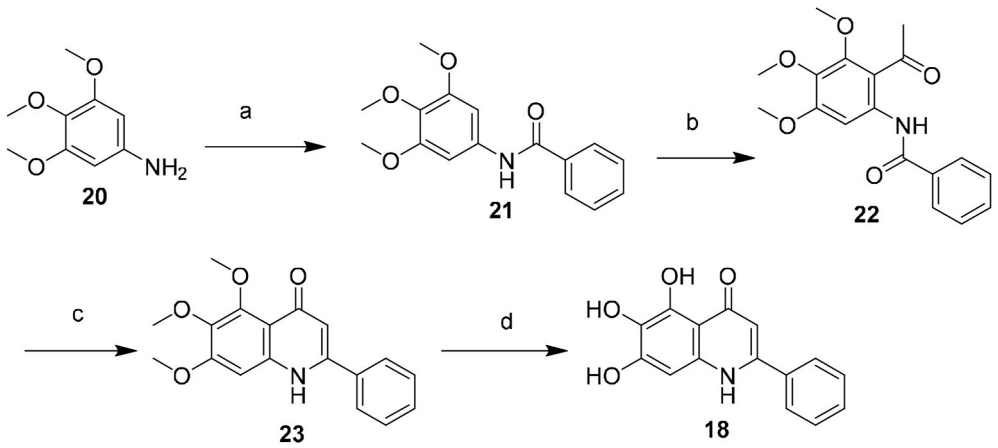

Scheme 1. Synthesis of compound **18**. Reagents and conditions: (a) benzoyl chloride, TEA, THF, 0 °C to rt, 2 h, 91%; (b) acetyl chloride, $SnCl_4$, anhydrous DCM, 0 °C to rt, 5 h, 45%; (c) KOH, anhydrous 1,4-dioxane, reflux, 4 h, 35%; (d) BBr_3/DCM, DCM, −10 °C to rt, 24 h, 75%.

and amines in the presence of PCl_3 in a good yield (Scheme 5) [33]. However, N_3-alkyl substituted compounds **D5** and **D12** could not be prepared with the synthetic method shown in Scheme 5, and these were obtained by a one-pot, two step cyclization: (i) the reaction of compound **36** with the prepared 2-phenylpropanoyl chloride or commercially available phenylacetyl chloride in the presence of triphenyl phosphite (TPP) and pyridine, and (ii) the substitution with isobutylamine [34], followed by demethylation (Scheme 6).

2.3. SAR studies of the quinazolin-4-one class of SARS-CoV-2 M^{pro} inhibitors

All target compounds were preliminarily evaluated for inhibitory activity against SARS-CoV-2 M^{pro} in fluorescence resonance energy transfer (FRET)-based enzymatic assays. As shown in Table 1, quinolin-4-one-based compound **18** had a complete loss of enzymatic inhibitory activity against SARS-CoV-2 M^{pro}. To our delight, quinazolin-4-one-based compound **19** was only slightly less potent than baicalein (IC_{50} = 1.372 ± 0.047 μM and 0.966 ± 0.065 μM, respectively). With the promising potency for compound **19** in hand, we firstly performed the SAR analysis of the substituents on the free phenyl group (C ring) in **19**. Generally, the positions on the phenyl ring led to this order of potency: 2′-position > 3′-position > 4′-position (Table 1). In particular, compounds with fluorine (F), trifluoromethyl (CF_3), trifluoromethoxy (OCF_3) or *tert*-butyl at the C2′ position exhibited much more potency than the corresponding compounds with 3′ and/or 4′ substituents (**A1** vs **A2** and **A3**, **A13** vs **A14**, **A15** vs **A16**, **A21** vs **A22**). The significant influence of the substituent position on activity can also be concluded from the difluorine-substituted compounds: 2′,3′-difluoro (**A25**, IC_{50} = 1.130 ± 0.031 μM) > 2′,4′-difluoro (**A26**, IC_{50} = 1.541 ± 0.042 μM) > 3′,4′-difluoro (**A27**, IC_{50} = 2.716 ± 0.051 μM).

The volume, polarity and electronegativity of the substituent groups also affect the potency significantly. Introduction of a bulky isopropyl (**A20**) and *tert*-butyl (**A21** and **A22**), or a polar hydroxyl (**A23** and **A24**) and a nitro group (**A17**–**A19**) resulted in a sharp decline in potency. It seemed that less bulky substituents with moderate-to-low electronegativity benefit the inhibitory activity against M^{pro}. **A10** with 2′-methyl and **A4** with 2′-chlorine were the two most active compounds among the A series, with IC_{50} values of 0.365 ± 0.033 μM and 0.435 ± 0.04 μM, respectively. Adding a bromine (Br) atom at the C2′ position, whose van der Waals radius is slightly larger than that of chlorine (Cl) atom and whose electronegativity is lower than that of Cl, led to compound **A7**, which showed a slightly decreased potency relative to **A4** (**A7**, IC_{50} = 0.554 ± 0.041 μM), but was more active than **19** and baicalein. The introduction of more electronegative substituents at the C2′ position led to a poorer potency against M^{pro}, for example, F (IC_{50} = 1.443 ± 0.060 μM) > CF_3 (IC_{50} = 1.481 ± 0.047 μM) > nitro group (IC_{50} = 10.588 ± 0.040 μM). Compound **A7** containing an electron-donating trifluoromethoxy (OCF_3) group was slightly less potent than compound **A13** with an electron-withdrawing CF_3 (IC_{50} = 1.798 ± 0.061 μM for **A7** vs 1.481 ± 0.047 μM for **A13**), which might be attributed to the larger volume of OCF_3 than that of CF_3, and the volume effect affected the potency more significantly. Together, these results suggested that the position, steric size, polarity and electronic property of substituents on the C ring integratedly affect the inhibitory activity against SARS-CoV-2 M^{pro}.

Next, we replaced the C ring with different types of groups in order to diversify the structures of quinazolin-4-one based M^{pro} inhibitors and search for more desirable substituents at the C2 position. As shown in the Table 2, the replacement of phenyl (the C ring) with naphthyl and heteroaromatic rings, including thienyl, 3-pyridyl, 4-pyridyl and pyrazolyl, led to compounds **B1**–**B5**, and resulted in a remarkable decrease in potency against M^{pro}. Different cycloalkyl replacements afforded compounds **B6**–**B8**. Substituting phenyl with cyclopentyl (**B7**, IC_{50} = 0.539 ± 0.061 μM) led to improved potency against M^{pro} over that of **19** (IC_{50} = 1.372 ± 0.047 μM) and baicalein (**14**) (IC_{50} = 0.966 ± 0.065 μM). **B8** with a cyclohexyl (IC_{50} = 1.370 ± 0.140 μM) was equipotent with **19**, while **B6** with cyclopropyl (IC_{50} = 5.485 ± 0.791 μM) remarkably decreased the potency. The phenyl was replaced by different alkyl groups leading to compounds **B9**–**B12**. The introduction of isopropyl (**B9**) and *tert*-butyl (**B10**) resulted in a sharp drop of the potency. In contrast, **B11** with *sec*-butyl (IC_{50} = 0.385 ± 0.024 μM) and **B12** with a bulkier *tert*-amyl (IC_{50} = 0.970 ± 0.075 μM) were more potent than or comparable to **19**, respectively. Subsequently, we explored the effects of styryl and benzyl groups at the C2 position on the inhibitory activity against M^{pro}. Compound **B13** with a rigid styryl (IC_{50} = 2.874 ± 0.030 μM) led to some loss of potency against M^{pro} compared to **19**. The relatively flexible benzyl group in compound **14** improved the IC_{50} value to 0.327 ± 0.052 μM. Small groups, such as methyl or ethyl, when introduced to the benzyl in **14** could further increase the activity, and the resulting compounds **15** and **16** exhibited the most potent inhibitory activity against M^{pro} among B series, with IC_{50} values of 0.174 ± 0.038 μM and 0.210 ± 0.028 μM, respectively. Addition of a larger isopropyl group (compound **17**) led to a slight loss of the potency of **14**, with an IC_{50} value of 0.390 ± 0.048 μM.

We tentatively kept R_2 as phenyl and explored the SAR at the N3 position (Table 3). Generally, C series compounds with different substituents at the N-3 position of quinazolin-4-one exhibited improved inhibitory potency against M^{pro} compared to compound **19** and baicalein (**14**), except for compounds **C2** with the polar hydroxyethyl (IC_{50} = 1.365 ± 0.062 μM), **C3** with a bulky *tert*-butyl (0.949 ± 0.077 μM) and **C14** with a biphenylyl (IC_{50} = 1.476 ± 0.117 μM). For cycloalkyl

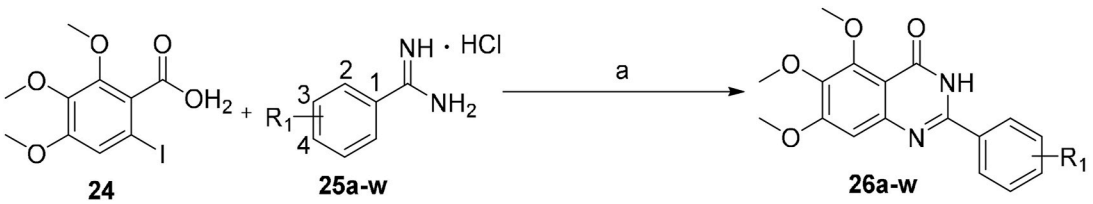

25a: R_1=2-F
25b: R_1=3-F
25c: R_1=4-F
25d: R_1=2-Cl
25e: R_1=3-Cl
25f: R_1=4-Cl
25g: R_1=3-Br
25h: R_1=4-Br
25i: R_1=2-CH_3
25j: R_1=3-CH_3
25k: R_1=4-CH_3
25l: R_1=3-CF_3
25m: R_1=4-OCF_3
25n: R_1=3-NO_2
25o: R_1=4-NO_2
25p: R_1=3-*tert*-butyl
25q: R_1=4-*tert*-butyl
25r: R_1=2-OH
25s: R_1=4-OH
25t: R_1=2,3-di-F
25u: R_1=2,4-di-F
25v: R_1=3,4-di-F
25w: R_1= H

26a: R_1=2-F
26b: R_1=3-F
26c: R_1=4-F
26d: R_1=2-Cl
26e: R_1=3-Cl
26f: R_1=4-Cl
26g: R_1=3-Br
26h: R_1=4-Br
26i: R_1=2-CH_3
26j: R_1=3-CH_3
26k: R_1=4-CH_3
26l: R_1=3-CF_3
26m: R_1=4-OCF_3
26n: R_1=3-NO_2
26o: R_1=4-NO_2
26p: R_1=3-*tert*-butyl
26q: R_1=4-*tert*-butyl
26r: R_1=2-OH
26s: R_1=4-OH
26t: R_1=2,3-di-F
26u: R_1=2,4-di-F
26v: R_1=3,4-di-F
26w: R_1=H

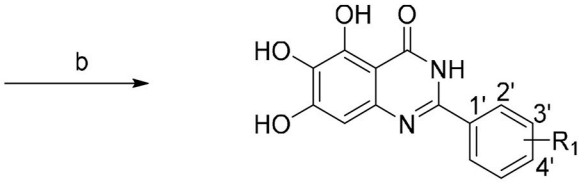

A1-A6, A8-A12, A14, A16, A18, A19, A21-A27 and 19

A1: R_1=2'-F
A2: R_1=3'-F
A3: R_1=4'-F
A4: R_1=2'-Cl
A5: R_1=3'-Cl
A6: R_1=4'-Cl
A8: R_1=3'-Br
A9: R_1=4'-Br
A10: R_1=2'-CH_3
A11: R_1=3'-CH_3
A12: R_1=4'-CH_3
A14: R_1=3'-CF_3
A16: R_1=4'-OCF_3
A18: R_1=3'-NO_2
A19: R_1=4'-NO_2
A21: R_1=3'-*tert*-butyl
A22: R_1=4'-*tert*-butyl
A23: R_1=2'-OH
A24: R_1=4'-OH
A25: R_1=2',3'-di-F
A26: R_1=2',4'-di-F
A27: R_1=3',4'-di-F
19: R_1=H

Scheme 2. Synthesis of compounds **A1**–**A6**, **A8**–**A12**, **A14**, **A16**, **A18**, **A19**, **A21**–**A27** and **19**. Reagents and conditions: (a) CuI, $CsCO_3$, DMF, rt, overnight, 55%–90%; (b) BBr_3/DCM, DCM, −10 °C to rt, 24–36 h, 35%–64%.

replacements, cyclopentyl was the optimal substituent group, and the corresponding compound **C5** showed significantly increased potency relative to **19**, with an IC_{50} value of 0.124 ± 0.014 μM (Table 3, Fig. S1). **C1** with a less bulky *sec*-butyl substituent showed potency as good as **C5** (Table 3, Fig. S1). The introduction of phenyl leading to compound **C7** improved the IC_{50} value to 0.085 ± 0.006 μM (Table 3, Fig. S1). Inspired by this result, different substituted phenyl groups were introduced to the N3 position. F, Br and hydroxyl substituents affording compounds **C8**–**C11** retained the most of the potency of **C7,** showing IC_{50} values of about 0.2 μM. Compound **C12** containing a 3′-methyl-4′-fluorophenyl substituent was equipotent with **C7** (IC_{50} = 0.117 ± 0.016 μM, Table 3, Fig. S1). In addition, adding a 3-pyridyl or 4-pyrazolyl at the N3 position resulted in compounds **C13** and **C14**, which had good inhibitory activity against M^{pro} (IC_{50} = 0.212 ± 0.024 and 0.390 ± 0.003 μM, respectively).

D series compounds were derived from the combination of the desirable substitutions at the C2 and N3 positions that we have identified (Table 4). Unexpectedly, the combination of 2-methyl-benzyl that is the optimal substitution at the C2 position with phenyl and *sec*-butyl groups that were the favorable substituents at the N3 position resulted in

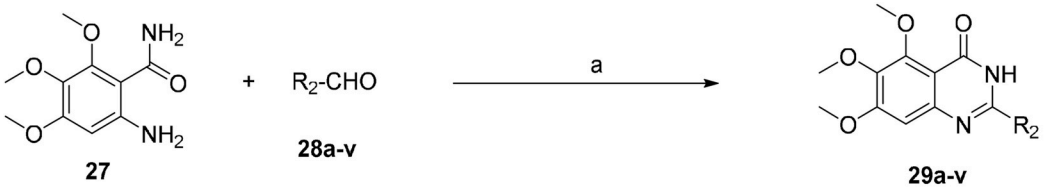

28a: R_2=2-Br-phenyl
28b: R_2=2-CF_3-phenyl
28c: R_2=2-OCF_3-phenyl
28d: R_2=2-NO_2-phenyl
28e: R_2=3-isopropyl-phenyl
28f: R_2=2-thienyl
28g: R_2=2-pyridyl
28h: R_2=4-pyridyl
28i: R_2= 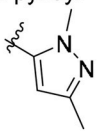
28j: R_2=naphthyl
28k: R_2=cyclopropyl
28l: R_2=cyclopentyl
28m: R_2=cyclohexyl
28n: R_2=isopropyl

28o: R_2=*tert*-butyl
28p: R_2=isobutyl
28q: R_2=*tert*-amyl
28r: R_2=styryl
28r: R_2= 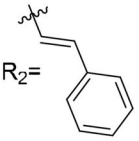
28s: R_2=benzyl
28t: R_2= 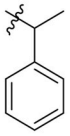
28u: R_2= 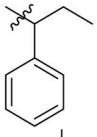
28v: R_2= 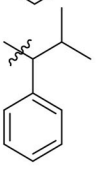

29a: R_2=2-Br-phenyl
29b: R_2=2-CF_3-phenyl
29c: R_2=2-OCF_3-phenyl
29d: R_2=2-NO_2-phenyl
29e: R_2=3-isopropyl-phenyl
29f: R_2=2-thienyl
29g: R_2=2-pyridyl
29h: R_2=4-pyridyl
29i: R_2= 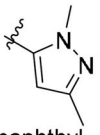
29j: R_2=naphthyl
29k: R_2=cyclopropyl
29l: R_2=cyclopentyl
29m: R_2=cyclohexyl
29n: R_2=isopropyl

29o: R_2=*tert*-butyl
29p: R_2=isobutyl
29q: R_2=*tert*-amyl
29r: R_2= 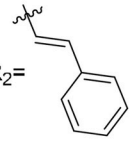
29s: R_2=benzyl
29t: R_2= 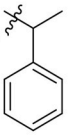
29u: R_2= 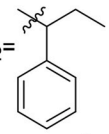
29v: R_2= 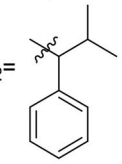

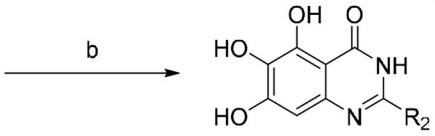

A7, A13, A15, A17, A20 and B1-B17

A7: R_2=2-Br-phenyl
A13: R_2=2-CF_3-phenyl
A15: R_2=2-OCF_3-phenyl
A17: R_2=2-NO_2-phenyl
A20: R_2=3-isopropyl-phenyl
B1: R_2=2-thienyl
B2: R_2=2-pyridyl
B3: R_2=4-pyridyl
B4: R_2= 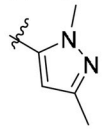

B5: R_2=naphthyl
B6: R_2=cyclopropyl
B7: R_2=cyclopentyl
B8: R_2=cyclohexyl
B9: R_2=isopropyl
B10: R_2=t*ert*-butyl
B11: R_2=isobutyl
B12: R_2=*tert*-amy
B13: R_2= 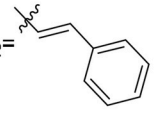
B14: R_2=benzyl

B15: R_2= 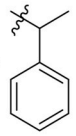
B16: R_2= 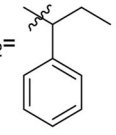
B17: R_2= 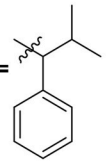

Scheme 3. Synthesis of compounds **A7**, **A13**, **A15**, **A17**, **A20**, **B1**–**B17**. Reagents and conditions: (a) I_2, EtOH, reflux, 3–5 h, 40%–80%; (b) BBr_3/DCM, DCM, −10 °C to rt, 24–36 h, 40%–63%.

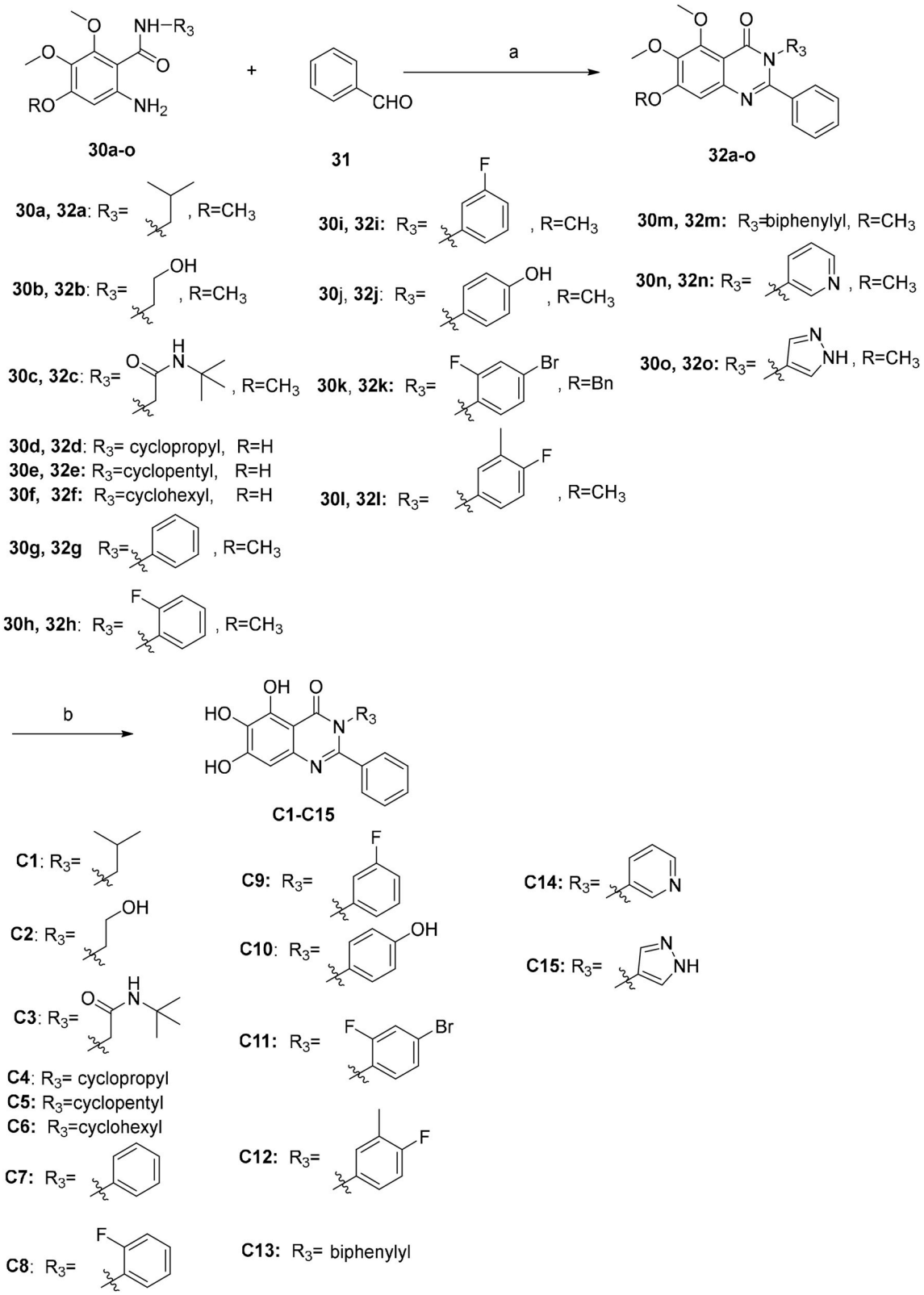

Scheme 4. Synthesis of compounds **C1**–**C15**. Reagents and conditions: (a) I_2, EtOH, reflux, 3–5 h, 45%–87%; (b) BBr_3/DCM, DCM, −10 °C to rt, 24–36 h, 35%–57%.

decreased activity compared to the corresponding **C** series compounds. In particular, compounds **D2** (IC_{50} = 1.005 ± 0.136 μM) and **D5** (IC_{50} = 0.692 ± 0.119 μM) showed a sharp decrease in potency relative to the corresponding compounds **C12** (IC_{50} = 0.117 ± 0.016 μM) and **C1** (IC_{50} = 0.124 ± 0.018 μM). The possible reason for the decreased inhibitory activity was that C_2-2-methyl-benzyl clashed with N_3-phenyl or N_3-*sec*-butyl, leading one or both of them to be unable to smoothly enter into the corresponding M^{pro} protein subpockets. N_3-*sec*-butyl series compounds **D6**–**D9** did not improve the potency compared to **C7**, with IC_{50} values ranging from 0.100 to 0.284 μM. The combination of C_2-benzyl

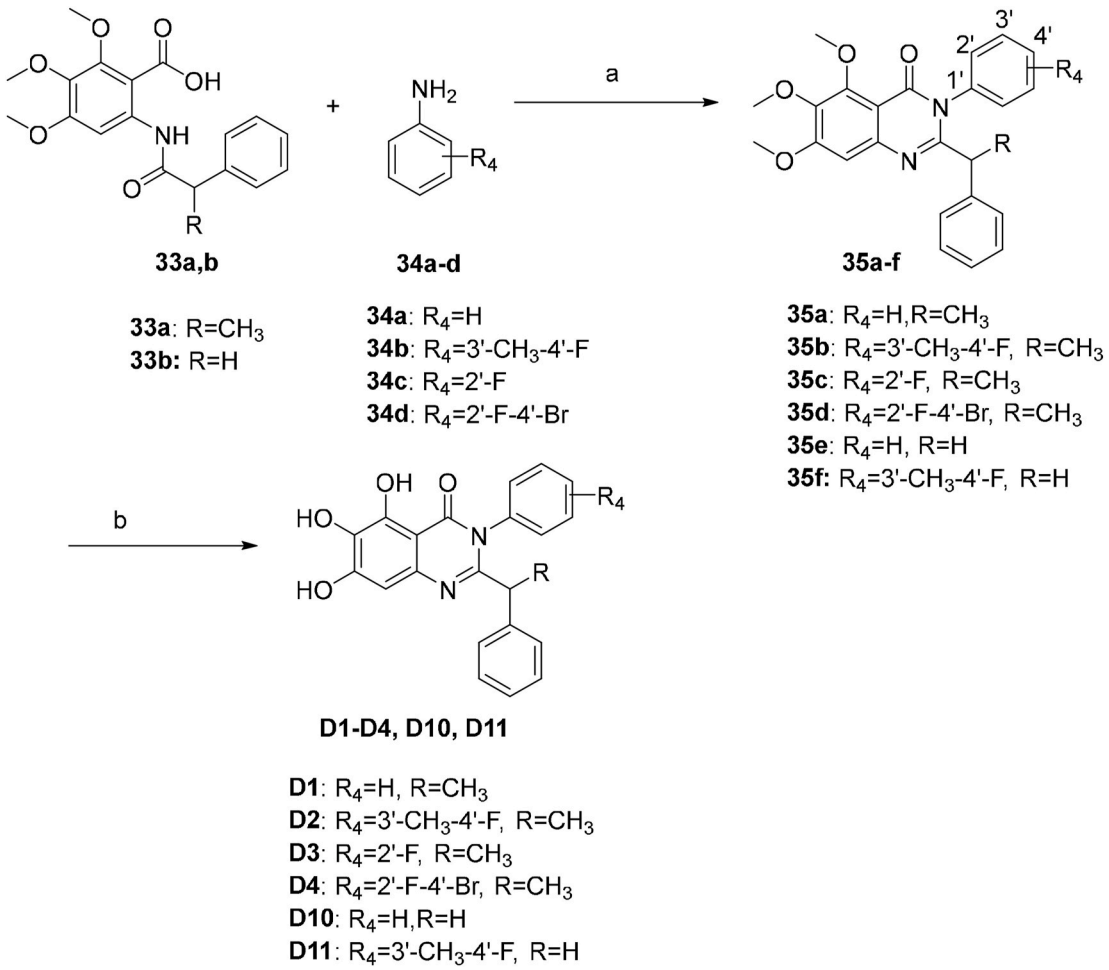

Scheme 5. Synthesis of compounds **D1**–**D4**, **D10** and **D11**. Reagents and conditions: (a) PCl_3, 50 °C, 4–12 h, 70%–82%; (b) BBr_3/DCM, DCM, −10 °C to rt, 24–36 h, 45%–63%.

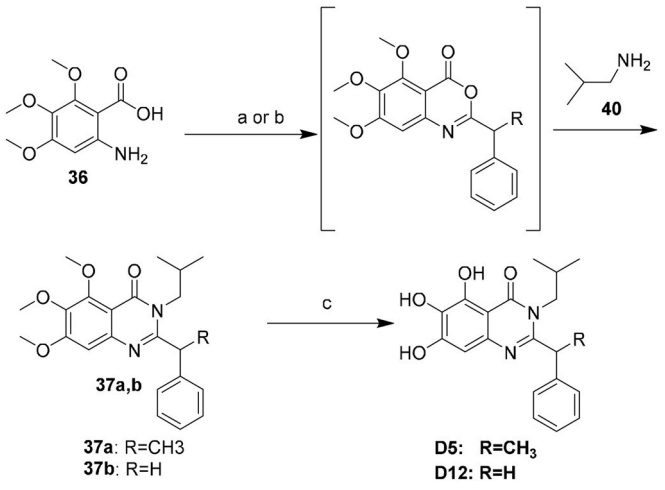

Scheme 6. Synthesis of compounds **D5** and **D12**. Reagents and conditions: (a) For **37a**: (i) 2-phenylpropanoic acid (**38**), $(COCl)_2$, DCM, cat. DMF, 0 °C to rt, 2 h; (ii) triphenyl phosphite (TPP), Py, 0 °C–70 °C, 2 h; iii) isobutylamine (**40**), 70 °C, overnight, 40%; (b) For **37b**: (i) phenylacetyl chloride (**39**), TPP, Py, 0 °C–70 °C, 2 h; (ii) isobutylamine (**40**), 70 °C, overnight, 45%; (c) BBr_3/DCM, DCM, −10 °C, 24 h, 50%–60%.

with N_3-phenyl resulted in compound **D10** being equipotent with **C7** (IC_{50} = 0.103 ± 0.014 μM), while the combination of C_2-benzyl with 3-methyl-4-fluorobenzyl and *sec*-butyl at the N3 position led to some loss of the potency relative to **C7**.

2.4. Target validation and selectivity

To examine if the inhibitory activity against M^{pro} is associated with covalent modification of cysteine residues, we compared the inhibition of **C5**, **C7**, **D6**, **D8** and **D10** in the presence or absence of the reducing agent dithiothreitol (DTT) (Table S1). Addition of DTT guarantees accessible cysteine residues of a protein at their reduced state and will indicate whether an inhibitor acts by a false mechanism of redox-cycling [24,35]. There were no significant differences in the IC_{50} values in the presence of DTT and in the absence of DTT.

One of the major limitations encountered by cysteine protease inhibitors is the target selectivity. Compound **C7** was selected as an example of our target scaffold to be profiled with the selectivity over several common human proteases, including caspase 2, cathepsin L, thrombin, cathepsin B and cathepsin D. Compound **C7** showed no apparent inhibitory activity against these host proteins at a concentration of 10 μM, suggesting that **C7** had a good target specificity against M^{pro} over host proteases (Table S2).

2.5. In vitro DMPK profiling

As shown in Table S3, compounds **C7** (Papp AB = 9.67×10^{-6} cm/s,

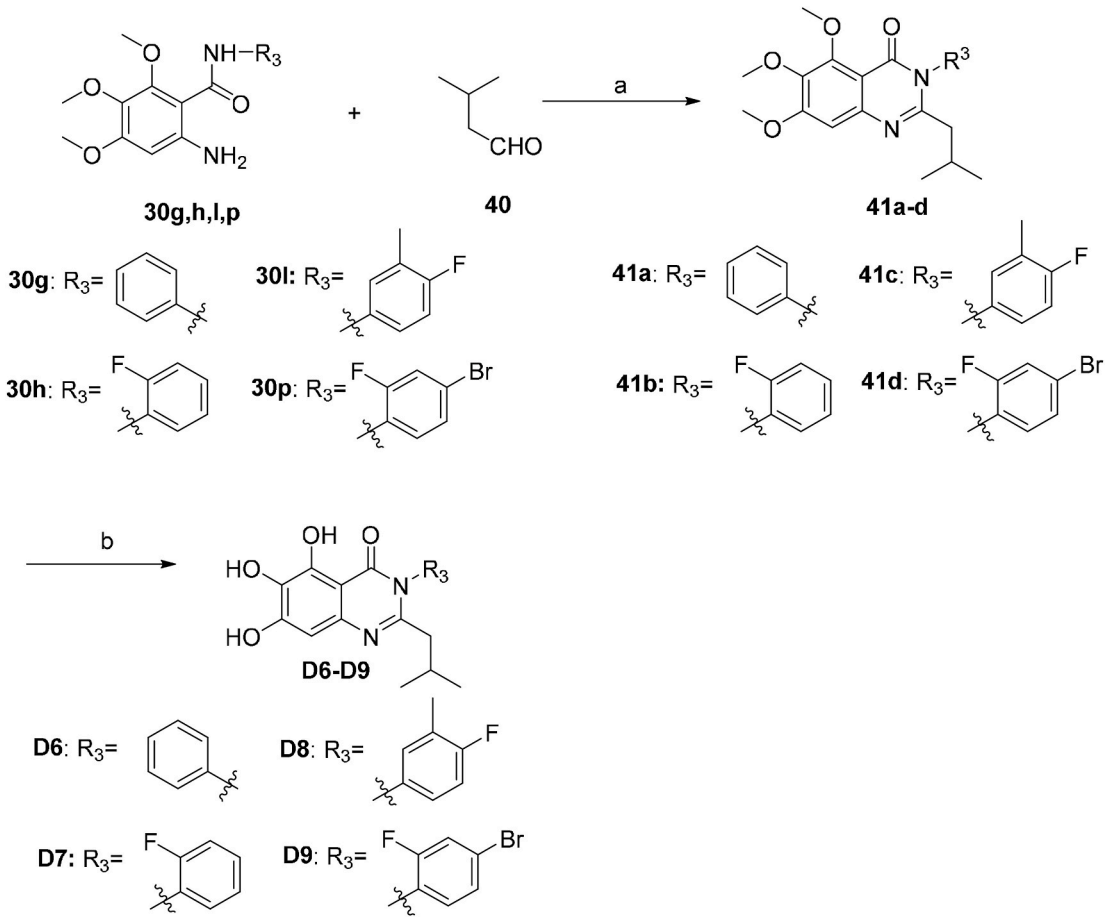

Scheme 7. Synthesis of compounds **D6**–**D9**. Reagents and conditions: (a) I_2, EtOH, reflux, 5 h, 72%–88%; (b) BBr_3/DCM, DCM, −10 °C to rt, 24 h, 55%–56%.

Efflux radio (ER) = 0.44), **D6** (Papp AB = 7.45×10^{-6} cm/s, ER = 0.40), and **D8** (Papp AB = 7.83×10^{-6} cm/s, ER = 0.41) exhibited improved Madin-Darby canine kidney (MDCK) membrane permeability relative to baicalein (Papp AB = 6.07×10^{-6} cm/s, ER = 0.34). The kinetic solubility in phosphate buffer solution (PBS, pH = 7.4) of **C7** and **D6** was measured as 179.35 and 155.98 μM, respectively, which were superior to baicalein (112.18 μM). **C7**, **D6**, **D8** and baicalein exhibited reasonable plasma protein binding (PPB) in human plasma (fraction unbound fu = 0.70%, 2.61%, 3.17% and 0.93%, respectively). Baicalein exhibited high intrinsic clearance in human liver microsome (HLM), with clearance rate (CL_{int}) of 333.05 μL/min/mg protein and half-time ($T_{1/2}$) of 4.16 min. **C7** and **D6** showed improved HLM stability relative to baicalein (CL_{int} = 108.68 and 68.34 μL/min/mg protein, respectively; $T_{1/2}$ = 12.75 and 20.28 min). The two compounds showed relatively high HLM metabolic stability in the presence of the cofactor NADPH alone, indicative of mainly undergoing phase II metabolism. With the presence of three phenolic hydroxyl groups in the structures, the above results were not unexpected. Despite the improvement relative to baicalein, the metabolic stability of this quinazolin-4-one series inhibitors requires further optimization.

2.6. Cellular cytotoxicity and antiviral activity

The antiviral activity of compounds **C7**, **D6** and **D8** was evaluated in SARS-CoV-2-infected Vero E6 cells. Prior to antiviral assays, the cytotoxicity of selected M^{pro} inhibitors against Vero E6 cells was evaluated by using cell counting kit-8 (CCK-8) assays. The test compounds exhibited no significant cytotoxicity at the highest tested concentration (50% cytotoxicity concentration, CC_{50} > 50 μM, Table 5 and Fig. S2). The antiviral activity was determined in a yield reduction assay that assesses the inhibitory activity of the test compounds on the viral replication using quantitative real-time polymerase chain reaction (qRT-PCR), with baicalein as the positive control. As shown in Table 5 and Fig. S2, compounds **C7** (EC_{50} = 1.10 ± 0.12 μM), **D6** (EC_{50} = 2.87 ± 1.43 μM) and **D8** (EC_{50} = 2.11 ± 1.12 μM) showed better antiviral activity in Vero E6 cells than baicalein (EC_{50} = 5.15 ± 1.64 μM).

2.7. X-ray crystal structure of *D8* in complex with SARS-CoV-2 M^{pro}

To further examine the binding mode of quinazolin-4-one inhibitors in SARS-CoV-2 M^{pro}, we resolved an X-ray co-crystal structure of **D8** complexed with M^{pro} at a resolution of 2.2 Å (PDB code 8I4S, Fig. 3A–**3C**). The X-ray data and refinement statistics are depicted in Table S4. The trihydroxyphenyl moiety of **D8** sits in a similar position as in the baicalein/M^{pro} complex (Fig. 3B and **E**). Three phenolic hydroxyl groups of **D8** form critical hydrogen bond interactions with the main chains of Gly143/Ser144/Gly145, and also form hydrogen bond interactions with the side chain of His163 *via* a buried water molecule (Fig. 3B). Distinct from the case of baicalein, the C4 carbonyl oxygen atom of **D8** was a little aside from Glu166, and forms a hydrogen bond with the backbone NH of Glu166 with the aid of a buried water molecule (Fig. 3B). Unexpectedly, the 3′-methyl-4′-fluorophenyl at the N3 position occupies the S2 pocket, forming hydrophobic interactions with Gln189 and Met49, while the *sec*-butyl at the C2 position projects into a newly formed binding site that was observed in CCF0058981 analogue (**12**) complexed with M^{pro} (PDB code 7LMF), termed the $S2_c$ pocket by Han et al. (Fig. 3D).[20] When **D8** bound to M^{pro}, the flexible side chains of some amino acid residues of the protein, particularly Met49 and Gln189, exhibited a ligand-induced conformation change relative to most other inhibitor/M^{pro} structures (*e.g.*, baicalein, nirmatrelvir and ensitrelvir),

Table 1
SAR exploration of the substituent groups on the C ring of quinazolin-4-one [a].

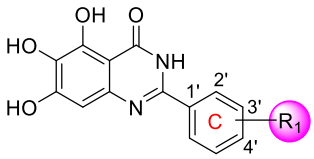

A series

Compd.	R_1	IC_{50} (μM)
A1	2′-F	1.443 ± 0.060
A2	3′-F	5.132 ± 0.094
A3	4′-F	12.760 ± 0.067
A4	2′-Cl	0.435 ± 0.041
A5	3′-Cl	6.960 ± 0.076
A6	4′-Cl	7.706 ± 0.055
A7	2′-Br	0.554 ± 0.041
A8	3′-Br	8.017 ± 0.033
A9	4′-Br	9.797 ± 0.051
A10	2′-methyl	0.365 ± 0.033
A11	3′-methyl	2.277 ± 0.029
A12	4′-methyl	1.867 ± 0.034
A13	2′-CF_3	1.481 ± 0.047
A14	3′-CF_3	10.53 ± 0.050
A15	2′-OCF_3	1.798 ± 0.061
A16	4′-OCF3	> 20
A17	2′-NO_2	10.588 ± 0.040
A18	3′-NO_2	11.169 ± 0.034
A19	4′-NO2	> 20
A20	3′-isopropyl	7.635 ± 0.058
A21	3′-*tert*-butyl	8.423 ± 0.031
A22	4′-*tert*-butyl	> 20
A23	2′-OH	18.285 ± 0.040
A24	4′-OH	> 20
A25	2′,3′-di-F	1.130 ± 0.031
A26	2′,4′-di-F	1.541 ± 0.042
A27	3,4′-di-F	2.716 ± 0.051
19	–	1.372 ± 0.047
baicalein (**14**)	–	0.966 ± 0.065

[a] Baicalein was used as the positive control. Inhibitory activity against SARS-CoV-2 $M^{pro}$was determined with the FRET protease activity assay. Values represent a mean ± SD of at least three independent experiments.

Table 2
SAR exploration of substituent groups at the C2 position of quinazolin-4-one[a].

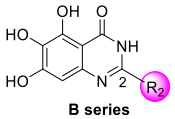

B series

Compd	R_2	IC_{50} (μM)
B1		> 20
B2		> 20
B3		15.19 ± 0.0405
B4		> 20
B5		3.565 ± 0.295
B6		5.485 ± 0.791
B7		0.539 ± 0.061
B8		1.370 ± 0.140
B9		4.943 ± 0.504
B10		4.086 ± 0.647
B11		0.385 ± 0.024
B12		0.970 ± 0.075
B13	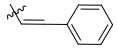	2.874 ± 0.030
B14		0.327 ± 0.052
B15		0.174 ± 0.038
B16		0.210 ± 0.028
B17	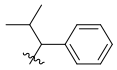	0.390 ± 0.048
19		1.372 ± 0.047
baicalein (14)	–	0.966 ± 0.065

[a] Baicalein was used as the positive control. Inhibitory activity against SARS-CoV-2 $M^{pro}$was determined by using the FRET protease activity assay. Values represent a mean ± SD of at least three independent experiments.

further rearranging the binding surface of subpockets S4 and S2 (Fig. 3D and **S3**). This allows the *sec*-butyl to occupy the S2c pocket, forming favorable hydrophobic interactions with Cys44, Thr45 and Ser46. As with baicalein, the phenyl ring of **D8** with three hydroxyl groups is sandwiched between Cys145 and Asn142 by forming S–π and NH_2-π with Cys145 and Asn142, respectively (Fig. 3B). In addition, the middle ring π–π stacks with catalytic His41, also contributing to the binding affinity of **D8** with protein (Fig. 3B).

Although highly conserved among variants of SARS-CoV-2, some mutated amino acid residues in M^{pro} have been observed, such as K90R in Beta strain B.1.351, K90R and A193V in Beta B.1.351.2, L205V in Zeta P.2, and P132H in Omicron B.1.529 [36]. However, it is worth noting that these amino residues are more than 10 Å away from the binding site of **D8** (Fig. S4), suggesting that **D8** should be have inhibitory effects against M^{pro} from SARS-CoV-2 variants. The assays assessing the inhibitory activity of the inhibitors against M^{pro} from SARS-CoV-2 Omicron variant are currently in progress.

3. Conclusions

M^{pro} has been validated as an effective target for development of orally available small molecule anti-COVID19 drugs. In this study, we sought to use medicinal chemistry and rational drug design approaches to structurally modify the first reported nonpeptidic, noncovalent SARS-CoV-2 M^{pro} inhibitor, baicalein. These efforts led to a series of quinazolin-4-one-derived noncovalent inhibitors with nanomolar potencies against SARS-CoV-2 M^{pro}. In particular, an optimized compound, **C7** exhibited superior inhibitory potency against M^{pro} relative to baicalein and is endowed with improved physicochemical and DMPK properties. Significantly, **C7** also showed more potent antiviral activity than baicalein (EC_{50} = 1.1 and 5.15 μM, respectively) in SARS-CoV-2-infected Vero E6 cells. Moreover, **C7** exhibited relatively high selectivity over a panel of human proteases (IC_{50} > 10 μM) and low cytotoxicity against Vero E6 cells (CC_{50} > 50 μM). The co-crystal structure of another potent inhibitor **D8** complexed with M^{pro} showed that the inhibitor noncovalently binds to the active site of M^{pro}, and occupies a newly formed S2c pocket that is not observed with baicalein and most

Table 3
SAR exploration of substituent groups at the N3 position of quinazolin-4-one[a].

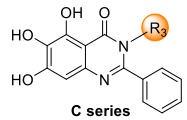

Compd	R_3	IC_{50} (μM)
C1		0.124 ± 0.018
C2		1.365 ± 0.062
C3		0.949 ± 0.077
C4		0.290 ± 0.028
C5		0.124 ± 0.016
C6		0.274 ± 0.022
C7		0.083 ± 0.006
C8		0.205 ± 0.033
C9		0.236 ± 0.018
C10	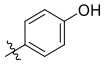	0.271 ± 0.018
C11	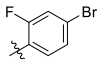	0.207 ± 0.024
C12		0.117 ± 0.016
C13	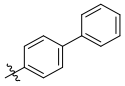	1.476 ± 0.117
C14		0.212 ± 0.024
C15		0.390 ± 0.003
19		1.372 ± 0.047
baicalein (14)	–	0.966 ± 0.065

[a] Baicalein was used as the positive control. Inhibitory activity against SARS-CoV-2 $M^{pro}$was determined by using the FRET protease activity assay. Values represent a mean ± SD of at least three independent experiments.

other M^{pro} inhibitors, and can be further exploited for inhibitor design. Meanwhile, the S1 and S4 subpocket remain largely unoccupied by **D8** and its analogues, leaving room for further improvement. While having improvements, the inhibitors still lack sufficient properties necessary to be profiled for *in vivo* antiviral efficacy in SARS-CoV-2-infected animal models. Further structural optimizations of this series of inhibitors are ongoing, and are focused on improving the DMPK properties, as well as further improving biochemical and cellular potencies. In addition, profiling the potency against M^{pro} from SARS-CoV-2 Omicron variant and other coronavirus is underway in our laboratory. Collectively, compound **C7** represents a promising lead for further development of more effective M^{pro} inhibitors and antiviral drugs against SARS-CoV-2 infection.

Table 4
SAR exploration of substituent groups at C-2 and N-3 positions of quinazolin-4-one[a].

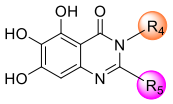

Compd	R_4	R_5	IC_{50} (μM)
D1			0.477 ± 0.078
D2			1.005 ± 0.136
D3			0.290 ± 0.030
D4	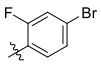		0.386 ± 0.017
D5			0.692 ± 0.119
D6			0.107 ± 0.023
D7			0.239 ± 0.028
D8			0.100 ± 0.012
D9	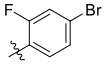		0.284 ± 0.028
D10			0.131 ± 0.022
D11			0.502 ± 0.038
D12			0.466 ± 0.040
C7			0.085 ± 0.006

[a] **C7** was used as the positive control. Inhibitory activity against SARS-CoV-2 $M^{pro}$was determined with the FRET protease activity assay. Values represent a mean ± SD of at least three independent experiments.

Table 5
Antiviral activity and cytotoxicity of selected compounds in Vero E6 cells.

Compd.	EC_{50} (μM)[a]	CC_{50} (μM)
C7	1.10 ± 0.12	> 50
D6	2.87 ± 1.43	> 50
D8	2.11 ± 1.16	> 50
baicalein	5.15 ± 2.46	> 50

[a] Inhibitory effect on viral replication induced by SARS-CoV-2 infection in Vero E6 cells (RT-qPCR assay). Values are expressed as mean ± SD from three independent experiments.

4. Experimental

4.1. Chemistry

Reagents and solvents from commercial sources were used without

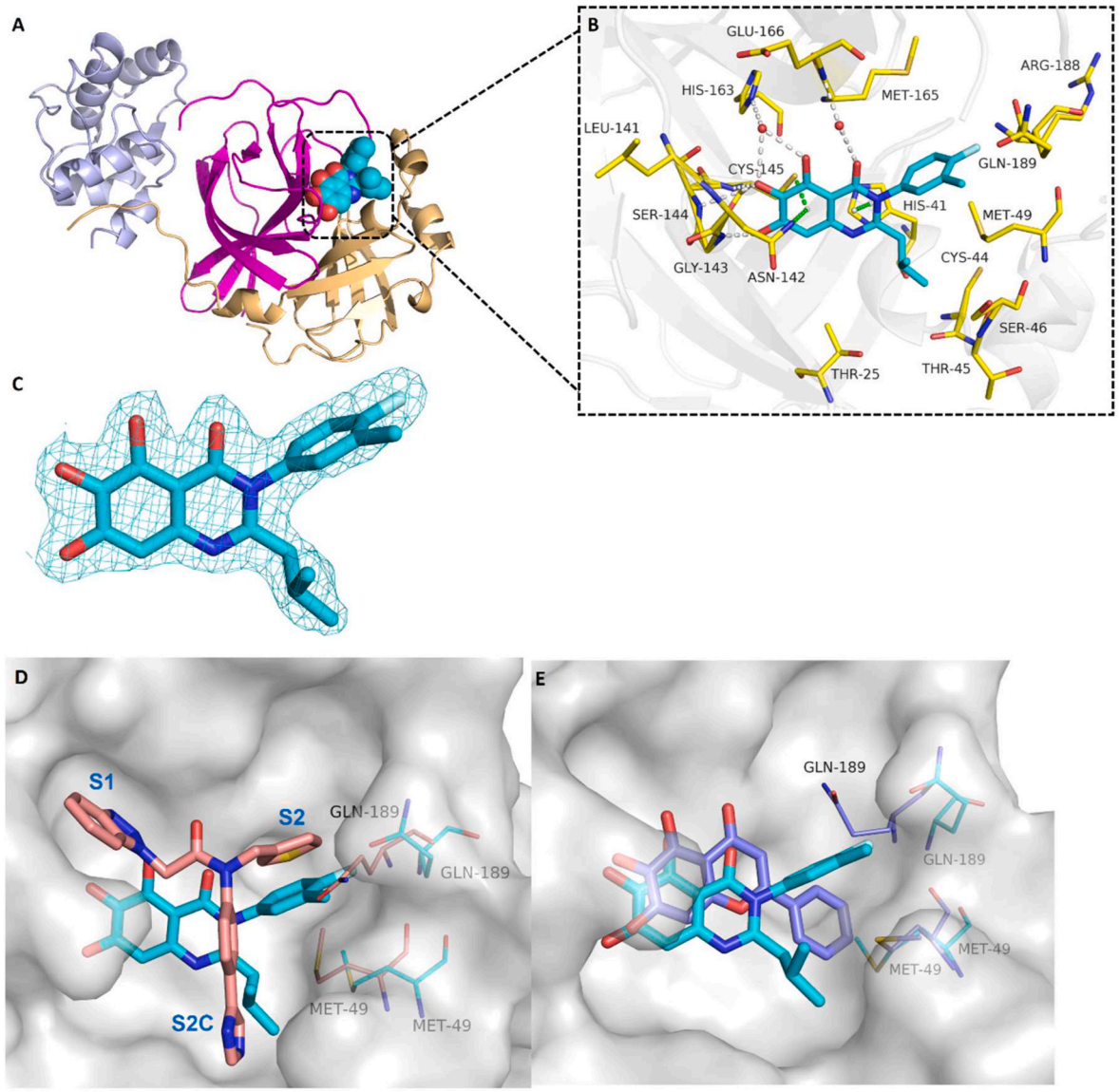

Fig. 3. (A) Overview of the co-crystal structure of **D8** bound to SARS-CoV-2 M^{pro} (PDB code 8I4S). The protein is shown in cartoon, and domains I, II and III are colored light orange, magenta and violet, respectively. **D8** is shown as spheres with carbons in cyan. (B) Detailed binding mode of compound **D8** in complex with SARS-CoV-2 M^{pro}. The protein is shown in gray cartoon, **D8** in cyan sticks, and the selected residues in yellow sticks. Hydrogen bonds are indicated as gray dashes, and the water molecule as a red sphere. S–π, NH_2–π and π–π stacks are indicated as green dashes. (C) *Fo*−*Fc* density map (contoured at 3.00σ) around **D8** (cyan mesh). (D) Overlay of **D8**/SARS-CoV-2 M^{pro} (PDB code 8I4S, cyan) with **12**/SARS-CoV-2 M^{pro} (PDB code 7LMF[20], pink) complexes, highlighting the residues Gln189 and Met49. (E) Overlay of **D8**/SARS-CoV-2 M^{pro} (cyan) with baicalein/SARS-CoV-2 M^{pro} (PDB code 6M2N[22], blue) complexes, highlighting the residues Gln189 and Met49.

further purification. The progress of all reactions was monitored by TLC using EtOAc/petroleum ether (PE) or dichloromethane (DCM)/MeOH as the solvent system, and spots were visualized by irradiation with UV light (254 nm) or by staining with phosphomolybdic acid. Flash chromatography was performed using silica gel (200−300 mesh). ^{1}H NMR and ^{13}C NMR spectra were recorded on a Bruker Avance ARX-400, a Bruker Avance ARX-500 or a Bruker Avance ARX-600. Chemical shifts δ are reported in ppm, and multiplicity of signals are denoted as: br = broad, s = singlet, d = doublet, t = triplet, q = quartet and m = multiplet. The low resolution ESI-MS was recorded on Shimadzu GCMS-2010 instruments and the high resolution mass spectra (HRMS) on a Water Q-Tofmicro mass spectrometer. Anhydrous DCM and *N*,*N*-dimethylformamide (DMF) were freshly distilled from calcium hydride. Anhydrous tetrahydrofuran (THF) was freshly distilled over sodium using benzophenone as the indicator. All other solvents were reagent grade. All moisture sensitive reactions were carried out in flame dried flasks under an argon atmosphere. The chemical purity of the target compounds was analyzed by high performance liquid chromatography (HPLC) on an InertSustain C18 column (4.6 mm × 250 mm, 5 μm) under gradient 60–100% MeOH in water (with 0.1% TFA in each mobile phase), with a flow rate of 1.0 mL/min and peak detection at 254 nm. All the target compounds showed purity greater than 95%. The synthesis and compound information of the intermediates can be found in the Supporting Information.

4.1.1. 5,6,7-Trihydroxy-2-phenylquinolin-4(1H)-one(**18**)

Step1: To the stirred solution of compound **20** (1.83 g, 10 mmol) in dry THF (25 mL) was added TEA (2 mL, 15 mmol) and benzoyl chloride (1.8 mL, 15 mmol) at 0 °C. Then the reaction mixture was stirred at room temperature (rt) for 2 h. The resulting mixture was concentrated and partitioned between water and DCM. The

combined organic layers were washed with brine, dried over anhydrous Na_2SO_4, filtered, and concentrated under the reduced pressure. The resulting residue triturated with *n*-hexane, filtered, washed with *n*-hexane, dried in vacuum to afford **21** as a white solid (2.61g, 91%), which was used directly in the next step without further purification.

Step2: To the stirred solution of compound **21** in anhydrous DCM (30 mL) was successively dropwise added acetyl chloride (0.78 mL, 11 mmol) and $SnCl_4$ (2 mL, 20 mmol) at 0 °C. The resulting reaction mixture was stirred at 0 °C for 4 h and then moved to room temperature for 1 h, after which the reaction mixture was poured into ice water. The aqueous portion was extracted with DCM (3 × 20 mL), and the combined organics were washed with brine, dried over anhydrous Na_2SO_4, filtered, and concentrated under reduced pressure. The residue was purified by silica column chromatography and eluted with petroleum ether: EtOAc (20:1) to give compound **22** as a white solid (1.48 g, 45%). ^{1}H NMR (400 MHz, $CDCl_3$) δ 12.37 (s, 1H), 8.42 (s, 1H), 8.05–7.99 (m, 2H), 7.59–7.47 (m, 3H), 4.00 (s, 6H), 3.85 (s, 3H), 2.67 (s, 3H). *m/z* (ESI-MS): 330.2 $[M + H]^+$.

Step3: To the stirred solution of compound **22** (1.32 g, 4.01 mmol) in anhydrous 1,4-dioxane (40 mL) was added NaOH (480 mg, 12 mmol), and the reaction mixture was heated to reflux under a nitrogen atmosphere for 4 h. Then, the reaction mixture was cooled to room temperature, and the solvent was removed under reduced pressure. Next, the residue was treated with water and *n*-hexane and the resulting mixture was sonicated for approximately 2 min. The resulting suspension was adjusted to pH~7 with 1 M HCl and filtered. The precipitate obtained was washed with *n*-hexane and dried under vacuum to afford compound **23** as a white solid (435 mg, 35%). ^{1}H NMR (400 MHz, $CDCl_3$) δ 8.07–8.01 (m, 2H), 7.96 (s, 1H), 7.54–7.45 (m, 3H), 7.02 (s, 1H), 4.21 (s, 3H), 4.05 (s, 3H), 3.95 (s, 3H). *m/z* (ESI-MS): 312.2 $[M + H]^+$.

Step4: To the stirred suspension of compound **23** (200 mg, 0.64 mmol) in anhydrous DCM (1.5 mL) was dropwise added BBr_3/DCM (9.6 mL, 9.6 mmol, 1 M) at −10 °C under a nitrogen atmosphere. The resulting reaction mixture was stirred at −10 °C overnight and then moved to room temperature for 12 h. Then, the mixture was moved to −10 °C again, and was quenched by slowly adding ice methanol, after which the solvent was removed under reduced pressure. The resulting residue was triturated with water, filtered, washed with water and DCM, dried in vacuum to afford **18** as a pale yellow solid (130 mg, 75%). ^{1}H NMR (400 MHz, DMSO-d_6) δ 14.02 (s, 1H), 11.26 (s, 1H), 9.31 (s, 1H), 8.04–7.95 (m, 2H), 7.67–7.57 (m, 3H), 7.32 (s, 1H), 7.03 (s, 1H). ^{13}C NMR (125 MHz, DMSO-d_6) δ 166.7, 156.1, 152.6, 139.2, 134.4, 132.2, 131.8, 131.5, 129.1, 128.5, 105.3, 101.1, 94.6. HRMS (ESI): *m/z* calcd for $C_{15}H_{10}NO_4$ $[M - H]^-$: 268.0615, found 268.0610. HPLC analysis: t_R = 10.216 min, 96.3%.

4.1.2. General procedure a for the preparation of A1–A6, A8 – A12, A14, A16, A18, A19, A21 – A27 and 19

Compound **24** (337 mg, 1 mmol) was dissolved in anhydrous DMF (6 mL), and compounds **25a**–**25w** (1.5 mmol), $CsCO_3$ (652 mg, 2 mmol) and CuI (39 mg, 0.2 mmol) were added. The resulting mixture was stirred at room temperature under nitrogen atmosphere overnight. After completion of the reaction, excess saturated aqueous NH_4Cl was added and filtered. The precipitate obtained was washed with a large amount of water, dried in vacuum to afford trimethoxyquinazolinones **26a**–**26w**.

To the stirred suspension of the obtained trimethoxyquinazolinone (0.5 mmol) in anhydrous DCM (1.5 mL) was dropwise added BBr_3/DCM (5 mL, 6 mmol, 1 M) at −10 °C under a nitrogen atmosphere. The resulting reaction mixture was stirred at −10 °C overnight and then moved to room temperature for 12–24 h. Then, the mixture was moved to −10 °C again, and was quenched by slowly adding ice methanol, after which the solvent was removed under the reduced pressure. The resulting residue was triturated with water, filtered, washed with water and DCM, dried in vacuum to afford target compounds **A1**–**A6**, **A8**–**A12**, **A14**, **A16**, **A18**, **A19**, **A21**–**A27** and **19**.

4.1.3. 5,6,7-Trihydroxy-2-phenylquinazolin-4(3H)-one (19)

The product was obtained as a offwhite solid (91 mg), yield 67%. ^{1}H NMR (400 MHz, DMSO-d_6) δ 12.46 (s, 1H), 11.76 (s, 1H), 10.33 (s, 1H), 8.91 (s, 1H), 8.10 (d, J = 6.7 Hz, 3H), 7.59–7.49 (m, 3H), 6.65 (s, 1H). ^{13}C NMR (125 MHz, DMSO-d_6) δ 166.4, 154.0, 149.4, 146.8, 142.1, 132.8, 131.1, 131.1, 128.6, 127.5, 103.2, 100.6. HRMS (ESI): *m/z* calcd for $C_{14}H_{11}N_2O_4$ $[M + H]^+$: 271.0713, found 271.0717. HPLC analysis: t_R = 6.765min, 96.9%.

4.1.4. 2-(2-Fluorophenyl)-5,6,7-trihydroxyquinazolin-4(3H)-one (A1)

According to general procedure A, the product was obtained as a white solid (65 mg), yield 45%. ^{1}H NMR (400 MHz, DMSO-d_6) δ 12.48 (s, 1H), 11.71 (s, 1H), 10.33 (s, 1H), 8.93 (s, 1H), 7.72 (t, J = 7.4 Hz, 1H), 7.63–7.56 (m, 1H), 7.41–7.31 (m, 2H), 6.63 (s, 1H). ^{13}C NMR (125 MHz, DMSO-d_6) δ 165.6, 159.5 (d, J = 250.2 Hz), 153.9, 146.8 (d, J = 6.8 Hz), 142.0, 132.6 (d, J = 8.5 Hz), 131.3, 131.0, 124.6 (d, J = 3.7 Hz), 122.2 (d, J = 13.1 Hz), 116.1 (d, J = 21.3 Hz), 103.2, 100.6. HRMS (ESI): *m/z* calcd for $C_{14}H_{10}FN_2O_4$ $[M + H]^+$: 289.0619, found 289.0623. HPLC analysis: t_R = 6.825 min, 95.3%.

4.1.5. 2-(3-Fluorophenyl)-5,6,7-trihydroxyquinazolin-4(3H)-one (A2)

According to general procedure A, the product was obtained as a white solid (68 mg), yield 47%. ^{1}H NMR (400 MHz, DMSO-d_6) δ 12.51 (br, 1H), 11.77 (s, 1H), 10.29 (s, 1H), 8.97 (s, 1H), 8.04–7.87 (m, 1H), 7.63–7.52 (m, 1H), 7.41 (td, J = 8.5, 2.6 Hz, 1H), 6.67 (s, 1H). ^{13}C NMR (125 MHz, DMSO-d_6) δ 166.6, 162.1 (d, J = 243.5 Hz), 154.0, 148.4, 146.8, 141.4, 135.0 (d, J = 8.1 Hz), 131.4, 130.7 (d, J = 8.4 Hz), 123.7 (d, J = 2.7 Hz), 118.0 (d, J = 21.0 Hz), 114.3 (d, J = 23.8 Hz), 103.0, 101.0. HRMS (ESI): *m/z* calcd for $C_{14}H_{10}FN_2O_4$ $[M + H]^+$: 289.0619, found 289.0622. HPLC analysis: t_R = 7.435 min, 95.5%.

4.1.6. 2-(4-Fluorophenyl)-5,6,7-trihydroxyquinazolin-4(3H)-one (A3)

According to general procedure A, the product was obtained as a white solid (56 mg), yield 39%. ^{1}H NMR (400 MHz, DMSO-d_6) δ 11.80 (s, 1H), 10.33 (s, 1H), 8.89 (br, 1H), 8.25–8.08 (m, 2H), 7.44–7.29 (m, 2H), 6.64 (s, 1H). ^{13}C NMR (125 MHz, DMSO-d_6) δ 166.7, 163.8 (d, J = 247.5 Hz), 153.9, 148.9, 146.8, 141.5, 131.0, 130.1 (d, J = 8.9 Hz), 129.2 (d, J = 2.9 Hz), 115.6 (d, J = 21.9 Hz), 102.7, 100.4. HRMS (ESI): *m/z* calcd for $C_{14}H_{10}FN_2O_4$ $[M + H]^+$: 289.0619, found 289.0617. HPLC analysis: t_R = 8.683 min, 98.9%.

4.1.7. 2-(2-Chlorophenyl)-5,6,7-trihydroxyquinazolin-4(3H)-one(A4)

According to general procedure A, the product was obtained as a white solid (90 mg), yield 59%. ^{1}H NMR (400 MHz, DMSO-d_6) δ 12.56 (s, 1H), 11.73 (s, 1H), 10.35 (s, 1H), 8.93 (s, 1H), 7.65–7.52 (m, 3H), 7.48 (td, J = 7.4, 1.5 Hz, 1H), 6.60 (s, 1H). ^{13}C NMR (150 MHz, DMSO-d_6) δ 165.5, 153.8, 149.1, 146.8, 141.7, 133.6, 131.6, 131.5, 131.2, 131.0, 129. 6, 127.2, 102.9, 100.7. HRMS (ESI): *m/z* calcd for $C_{14}H_{10}ClN_2O_4$ $[M + H]^+$: 305.0324, found 305.0323. HPLC analysis: t_R = 6.920 min, 95.2%.

4.1.8. 2-(3-Chlorophenyl)-5,6,7-trihydroxyquinazolin-4(3H)-one (A5)

According to general procedure A, the product was obtained as a white solid (94 mg), yield 62%. ^{1}H NMR (400 MHz, DMSO-d_6) δ 12.50 (br, 1H), 11.73 (s, 1H), 10.35 (br, 1H), 8.98 (br, 1H), 8.16 (t, J = 1.9 Hz, 1H), 8.07 (d, J = 7.9 Hz, 1H), 7.69–7.48 (m, 2H), 6.67 (s, 1H). ^{13}C NMR (125 MHz, DMSO-d_6) δ 166.5, 153.9, 148.2, 146.8, 141.7, 134.8, 133.4, 131.4, 130.8, 130.5, 127.3, 126.2, 103.4, 100.7. HRMS (ESI): *m/z* calcd for $C_{14}H_{10}ClN_2O_4$ $[M + H]^+$: 305.0324, found 305.0323. HPLC analysis: t_R = 12.106 min, 96.2%.

4.1.9. 2-(4-Chlorophenyl)-5,6,7-trihydroxyquinazolin-4(3H)-one (A6)

According to general procedure A, the product was obtained as a

white solid (97 mg), yield 64%. ^{1}H NMR (400 MHz, DMSO-d_6) δ 12.51 (s, 1H), 11.72 (s, 1H), 10.36 (s, 1H), 8.94 (s, 1H), 8.15–8.09 (m, 2H), 7.62–7.56 (m, 2H), 6.64 (s, 1H). ^{13}C NMR (125 MHz, DMSO-d_6) δ 166.3, 154.0, 148.4, 146.8, 141.9, 135.9, 131.6, 131.3, 129.3, 128.7, 103.3, 100.6. HRMS (ESI): *m/z* calcd for $C_{14}H_{10}ClN_2O_4$ $[M + H]^+$: 305.0324, found 305.0317. HPLC analysis: t_R = 9.457 min, 98.0%.

4.1.10. 2-(3-Bromophenyl)-5,6,7-trihydroxyquinazolin-4(3H)-one (A8)

According to general procedure A, the product was obtained as a white solid (104 mg), yield 60%. ^{1}H NMR (400 MHz, DMSO-d_6) δ 12.54 (br, 1H), 11.78 (s, 1H), 10.37 (s, 1H), 8.96 (s, 1H), 8.29 (s, 1H), 8.11 (d, J = 7.9 Hz, 1H), 7.76 (d, J = 7.8 Hz, 1H), 7.49 (t, J = 7.9 Hz, 1H), 6.66 (s, 1H). ^{13}C NMR (125 MHz, DMSO-d_6) δ 166.6, 153.9, 148.3, 146.8, 141.3, 134.9, 133.7, 131.3, 130.7, 130.1, 126.5, 121.9, 102.9, 100.6. HRMS (ESI): *m/z* calcd for $C_{14}H_{10}^{79}BrN_2O_4$ $[M + H]^+$: 348.9819, found 348.9823. HPLC analysis: t_R = 10.440 min, 95.4%.

4.1.11. 2-(4-Bromophenyl)-5,6,7-trihydroxyquinazolin-4(3H)-one (A9)

According to general procedure A, the product was obtained as a white solid (108 mg), yield 62%. ^{1}H NMR (400 MHz, DMSO-d_6) δ 12.51 (s, 1H), 11.77 (s, 1H), 10.35 (s, 1H), 8.94 (s, 1H), 8.09–8.02 (m, 2H), 7.780–7.71 (m, 2H), 6.65 (s, 1H). ^{13}C NMR (125 MHz, DMSO-d_6) δ 166.6, 153.9, 148.8, 146. 8, 141.5, 131.9, 131.6, 131.2, 129.5, 124.8, 102.8, 100.6. HRMS (ESI): *m/z* calcd for $C_{14}H_8^{79}BrN_2O_4$ $[M - H]^-$: 346.9673, found 346.9666. HPLC analysis: t_R = 11.866 min, 96.6%.

4.1.12. 5,6,7-Trihydroxy-2-(o-tolyl)quinazolin-4(3H)-one (A10)

According to general procedure A, the product was obtained as a white solid (50 mg), yield 35%. ^{1}H NMR (400 MHz, DMSO-d_6) δ 12.37 (s, 1H), 11.78 (s, 1H), 10.28 (s, 1H), 8.87 (s, 1H), 7.47–7.38 (m, 2H), 7.35–7.28 (m, 2H), 6.58 (s, 1H), 2.35 (s, 3H). ^{13}C NMR (150 MHz, DMSO-d_6) δ 166.3, 153.8, 151.7, 146.8, 141.3, 136.2, 134.0, 131.0, 130.5, 129.8, 129.2, 125.7, 102.8, 100.5, 19.6. HRMS (ESI): *m/z* calcd for $C_{15}H_{11}N_2O_4$ $[M - H]^-$: 283.0724, found 283.0718. HPLC analysis: t_R = 9.143 min, 99.2%.

4.1.13. 5,6,7-Trihydroxy-2-(m-tolyl)quinazolin-4(3H)-one (A11)

According to general procedure A, the product was obtained as a white solid (57 mg), yield 40%. ^{1}H NMR (400 MHz, DMSO-d_6) δ 11.84 (br, 1H), 10.36 (s, 1H), 8.90 (br, 1H), 7.93 (s, 1H), 7.88 (d, J = 7.5 Hz, 1H), 7.45–7.34 (m, 2H), 6.65 (s, 1H), 2.39 (s, 3H). ^{13}C NMR (125 MHz, DMSO-d_6) δ 166.8, 153.9, 150.1, 146.8, 141.5, 137.9, 132.5, 131.8, 131.0, 128.5, 128.1, 124.7, 102.6, 100.5, 21.0. HRMS (ESI): *m/z* calcd for $C_{15}H_{11}N_2O_4$ $[M - H]^-$: 283.0724, found 283.0722. HPLC analysis: t_R = 7.412 min, 95.1%.

4.1.14. 5,6,7-Trihydroxy-2-(p-tolyl)quinazolin-4(3H)-one (A12)

According to general procedure A, the product was obtained as a white solid (61 mg), yield 43%. ^{1}H NMR (400 MHz, DMSO-d_6) δ 12.38 (br, 1H), 11.82 (s, 1H), 10.31 (s, 1H), 8.87 (s, 1H), 8.05–7.98 (m, 2H), 7.36–7.30 (m, 2H), 6.62 (s, 1H), 2.38 (s, 3H). ^{13}C NMR (125 MHz, DMSO-d_6) δ 166.8, 154.4, 150.1, 147.3, 141.6, 131.3, 130.3, 129.6, 127.9, 102.7, 100.9, 21.42. HRMS (ESI): *m/z* calcd for $C_{15}H_{11}N_2O_4$ $[M - H]^-$: 283.0724, found 283.0717. HPLC analysis: t_R = 5.061 min, 97.0%.

4.1.15. 5,6,7-Trihydroxy-2-(3-(trifluoromethyl)phenyl)quinazolin-4(3H)-one (A14)

According to general procedure A, the product was obtained as a white solid (68 mg), yield 40%. ^{1}H NMR (400 MHz, DMSO-d_6) δ 12.68 (s, 1H), 11.72 (s, 1H), 10.38 (s, 1H), 8.99 (s, 1H), 8.46 (s, 1H), 8.41 (d, J = 8.1 Hz, 1H), 7.93 (d, J = 7.7 Hz, 1H), 7.77 (t, J = 7.8 Hz, 1H), 6.68 (s, 1H). ^{13}C NMR (150 MHz, DMSO-d_6) δ 166.3, 154.0, 148.0, 146.7, 141.8, 133.7, 131.53, 131.45, 129.8, 129.4 (q, J = 32.0 Hz), 127.5, 124.2, 124.0 (q, J = 272.3 Hz), 103.4, 100.7. HRMS (ESI): *m/z* calcd for $C_{15}H_8F_3N_2O_4$ $[M - H]^-$: 337.0442, found 337.0436. HPLC analysis: t_R = 8.083 min, 97.2%.

4.1.16. 5,6,7-Trihydroxy-2-(4-(trifluoromethoxy)phenyl)quinazolin-4(3H)-one (A16)

According to general procedure A, the product was obtained as a yellow solid (76 mg), yield 43%. ^{1}H NMR (400 MHz, DMSO-d_6) δ 11.78 (br, 1H), 10.35 (br, 1H), 8.27–8.18 (m, 2H), 7.56–7.49 (m, 2H), 6.66 (s, 1H). ^{13}C NMR (125 MHz, DMSO-d_6) δ 166.5, 158.2, 153.9, 150.2, 148.6, 146.8, 141.4, 131.8, 131.2, 129.8, 128.3, 120.8, 120.0 (q, J = 257.4 Hz), 102.7, 100.5. HRMS (ESI): *m/z* calcd for $C_{15}H_8F_3N_2O_5$ $[M - H]^-$: 353.0391, found 353.0381. HPLC analysis: t_R = 8.742 min, 96.3%.

4.1.17. 5,6,7-Trihydroxy-2-(3-nitrophenyl)quinazolin-4(3H)-one (A18)

According to general procedure A, the product was obtained as a yellow solid (71 mg), yield 45%. ^{1}H NMR (400 MHz, DMSO-d_6) δ 12.76 (s, 1H), 11.71 (s, 1H), 10.42 (s, 1H), 9.02 (s, 1H), 8.94 (s, 1H), 8.53 (d, J = 7.8 Hz, 1H), 8.38 (dd, J = 8.2, 2.2 Hz, 1H), 7.81 (t, J = 8.0 Hz, 1H), 6.69 (s, 1H). ^{13}C NMR (125 MHz, DMSO-d_6) δ 167.0, 154.4, 148.4, 147.8, 147.2, 141.9, 134.7, 134.2, 132.0, 130.7, 125.9, 122.8, 103.9, 101.2. HRMS (ESI): *m/z* calcd for $C_{14}H_8N_3O_6$ $[M - H]^-$: 314.0419, found 314.0412. HPLC analysis: t_R = 11.254 min, 97.5%.

4.1.18. 5,6,7-Trihydroxy-2-(4-nitrophenyl)quinazolin-4(3H)-one (A19)

According to general procedure A, the product was obtained as a yellow solid (61 mg), yield 39%. ^{1}H NMR (400 MHz, DMSO-d_6) δ 12.74 (s, 1H), 11.70 (s, 1H), 10.44 (s, 1H), 9.07 (s, 1H), 8.41–8.30 (s, 4H), 6.70 (s, 1H). ^{13}C NMR (125 MHz, DMSO-d_6) δ 166.1, 153.9, 148.7, 147.6, 146.7, 141.6, 138.5, 131.8, 128.9, 123.6, 103.6, 100.7. HRMS (ESI): *m/z* calcd for $C_{14}H_8N_3O_6$ $[M - H]^-$: 314.0419, found 314.0412. HPLC analysis: t_R = 8.392 min, 97.7%.

4.1.19. 2-(3-(tert-Butyl)phenyl)-5,6,7-trihydroxyquinazolin-4(3H)-one (A21)

According to general procedure A, the product was obtained as a white solid (68 mg), yield 42%. ^{1}H NMR (400 MHz, DMSO-d_6) δ 12.53 (br, 1H), 11.84 (s, 1H), 10.37 (s, 1H), 8.89 (s, 1H), 8.10 (s, 1H), 7.92 (d, J = 8.0 Hz, 1H), 7.58 (d, J = 7.9 Hz, 1H), 7.45 (t, J = 7.8 Hz, 1H), 6.66 (s, 1H), 1.34 (s, 9H). ^{13}C NMR (150 MHz, DMSO-d_6) δ 166.9, 153.9, 151.1, 150.0, 146.8, 141.4, 132.4, 131.0, 128.4, 128.1, 125.0, 124.3, 102.5, 100.5, 34.8, 31.1.

HRMS (ESI): *m/z* calcd for $C_{18}H_{17}N_2O_4$ $[M - H]^-$: 325.1194, found 325.1189. HPLC analysis: t_R = 12.850 min, 95.2%.

4.1.20. 2-(4-(tert-Butyl)phenyl)-5,6,7-trihydroxyquinazolin-4(3H)-one (A22)

According to general procedure A, the product was obtained as a white solid (67 mg), yield 41%. ^{1}H NMR (400 MHz, DMSO-d_6) δ 12.38 (s, 1H), 11.80 (s, 1H), 10.29 (s, 1H), 8.85 (s, 1H), 8.10–8.01 (m, 2H), 7.56–7.51 (m, 2H), 6.63 (s, 1H), 1.32 (s, 9H). ^{13}C NMR (150 MHz, DMSO-d_6) δ 166.3, 153.9, 149.6, 146.8, 142.2, 130. 9, 130.0, 128.6, 127.3, 125.4, 102.9, 100.5, 34.7, 30.9. HRMS (ESI): *m/z* calcd for $C_{18}H_{17}N_2O_4$ $[M - H]^-$: 325.1194, found 325.1185. HPLC analysis: t_R = 10.744 min, 97.0%.

4.1.21. 5,6,7-Trihydroxy-2-(2-hydroxyphenyl)quinazolin-4(3H)-one (A23)

According to general procedure A, the product was obtained as a white solid (50 mg), yield 35%. ^{1}H NMR (400 MHz, DMSO-d_6) δ 13.71 (br, 1H), 12.42 (br, 1H), 11.60 (s, 1H), 10.48 (s, 1H), 9.03 (s, 1H), 8.15 (dd, J = 8.1, 1.6 Hz, 1H), 7.47–7.37 (m, 1H), 7.01–6.92 (m, 2H), 6.63 (s, 1H). ^{13}C NMR (125 MHz, DMSO-d_6) δ 165.4, 159.8, 154.2, 151.1, 147.0, 139.0, 133.4, 131.4, 127.4, 118.8, 117.8, 113.8, 101.8, 100.4. HRMS (ESI): *m/z* calcd for $C_{14}H_9N_2O_5$ $[M - H]^-$: 285.0517, found 285.0509. HPLC analysis: t_R = 9.255 min, 95.4%.

4.1.22. 5,6,7-Trihydroxy-2-(4-hydroxyphenyl)quinazolin-4(3H)-one (**A24**)

According to general procedure A, the product was obtained as a white solid (54 mg), yield 38%. ^{1}H NMR (300 MHz, DMSO-d_6) δ 12.27 (br, 1H), 11.85 (s, 1H), 10.27 (s, 1H), 10.13 (s, 1H), 8.81 (s, 1H), 8.06–7.93 (m, 2H), 6.93–6.82 (m, 2H), 6.58 (s, 1H). ^{13}C NMR (150 MHz, DMSO-d_6) δ 166.4, 160.3, 154.0, 149.2, 146.8, 142.4, 130.5, 129.3, 123.3, 115.3, 102.5, 100.2. HRMS (ESI): *m/z* calcd for $C_{14}H_9N_2O_5$ [M − H] $^-$: 285.0517, found 285.0514. HPLC analysis: t_R = 10.262 min, 96.1%.

4.1.23. 2-(2,3-Difluorophenyl)-5,6,7-trihydroxyquinazolin-4(3H)-one (**A25**)

According to general procedure A, the product was obtained as a white solid (77 mg), yield 50%. ^{1}H NMR (400 MHz, DMSO-d_6) δ 12.60 (s, 1H), 11.67 (s, 1H), 10.40 (s, 1H), 9.01 (s, 1H), 7.69–7.60 (m, 1H), 7.58–7.51 (m, 1H), 7.40–7.32 (m, 1H), 6.64 (s, 1H). ^{13}C NMR (125 MHz, DMSO-d_6) δ 166.0, 154.35, 151.17 (d, J = 12.5 Hz), 149.17 (dd, J = 13.2, 9.5 Hz), 147.20, 146.07 (d, J = 3.5 Hz), 142.26, 132.04, 126.60 (d, J = 3.5 Hz), 125.88–125.24 (m), 124.68 (d, J = 9.6 Hz), 119.93 (d, J = 17.3 Hz), 103.9, 101.1. HRMS (ESI): *m/z* calcd for $C_{14}H_7F_2N_2O_4$ [M − H] $^-$: 305.0379, found 305.0369. HPLC analysis: t_R = 8.571 min, 96.1%.

4.1.24. 2-(2,4-Difluorophenyl)-5,6,7-trihydroxyquinazolin-4(3H)-one (**A26**)

According to general procedure A, the product was obtained as a white solid (84 mg), yield 55%. ^{1}H NMR (400 MHz, DMSO-d_6) δ 12.52 (s, 1H), 11.69 (s, 1H), 10.36 (s, 1H), 8.97 (s, 1H), 7.83–7.76 (m, 1H), 7.50–7.42 (m, 1H), 7.25 (td, J = 8.5, 2.5 Hz, 1H), 6.62 (s, 1H). ^{13}C NMR (125 MHz, DMSO-d_6) δ 165.6, 163.5 (dd, J = 248.8, 11.3Hz), 160.0 (J = 253.2, 12.6 Hz), 153.9, 146.7, 146.0, 141.9, 132.6 (dd, J = 10.6, 3.7 Hz), 131.4, 119.0 (dd, J = 13.1, 3.5 Hz), 111.9 (dd, J = 22.1, 3.1 Hz), 104.6 (t, J = 26.0 Hz), 103.2, 100.6. HRMS (ESI): *m/z* calcd for $C_{14}H_7F_2N_2O_4$ [M − H] $^-$: 305.0379, found 305.0369. HPLC analysis: t_R = 7.082 min, 95.4%.

4.1.25. 2-(3,4-Difluorophenyl)-5,6,7-trihydroxyquinazolin-4(3H)-one (**A27**)

According to general procedure A, the product was obtained as a white solid (77 mg), yield 50%. ^{1}H NMR (400 MHz, DMSO-d_6) δ 12.53 (s, 1H), 11.69 (s, 1H), 10.38 (s, 1H), 8.97 (s, 1H), 8.20–8.13 (m, 1H), 8.04–7.97 (m, 1H), 7.67–7.57 (m, 1H), 6.65 (s, 1H). ^{13}C NMR (125 MHz, DMSO-d_6) δ 165.6 (d, J = 141.3 Hz), 153.9, 152.2 (d, J = 13.4 Hz), 150.2 (t, J = 12.7 Hz), 148.3 (d, J = 12.9 Hz), 147.3, 146.7, 141.7, 131.32, 130.2 (dd, J = 6.2, 3.4 Hz), 124.84, 117.79 (d, J = 17.7 Hz), 116.76 (d, J = 19.3 Hz), 103.3, 100.5. HRMS (ESI): *m/z* calcd for $C_{14}H_7F_2N_2O_4$ [M − H] $^-$: 305.0379, found 305.0371. HPLC analysis: t_R = 7.863 min, 95.4%.

4.1.26. General procedure B for the preparation of compounds A7, A13, A15, A17, A20, B1–B17, C1–C15 and D6–D9

To the stirred solution of **27** or **30a**–**30p** (1 mmol) in anhydrous EtOH (10 mL) was added I_2 (1.2 mmol) and the corresponding aldehyde (1.2 mmol). The resulting reaction mixture was heated to reflux and stirred for 3–5 h. After completion of the reaction, the reaction mixture was cooled to room temperature and was quenched with excess 5% aqueous $Na_2S_2O_3$. The aqueous portion was extracted with DCM (3 × 10 mL), and the combined organic layers were washed with brine, dried over anhydrous Na_2SO_4, filtered, and concentrated under reduced pressure. The residue was purified by silica column chromatography (DCM/MeOH = 300:1 to 150:1) to give the corresponding quinazolinones **29a**–**29v**, **32a**–**32o**, and **41a**–**41d**.

According to general procedure A, the demethylation of the above quinazolinones afforded the target compounds **A7**, **A13**, **A15**, **A17**, **A20**, **B1**–**B17**, **C1**–**C15** and **D6**–**D9**.

4.1.27. 2-(2-Bromophenyl)-5,6,7-trihydroxyquinazolin-4(3H)-one (**A7**)

According to general procedure B, the product was obtained as a white solid (99 mg), yield 57%. ^{1}H NMR (400 MHz, DMSO-d_6) δ 12.55 (s, 1H), 11.76 (s, 1H), 10.36 (s, 1H), 8.94 (s, 1H), 7.76 (dd, J = 7.7, 1.5 Hz, 1H), 7.60 (dd, J = 7.4, 2.1 Hz, 1H), 7.56–7.42 (m, 2H), 6.60 (s, 1H). ^{13}C NMR (125 MHz, DMSO-d_6) δ 165.5, 153.8, 150.2, 146.8, 141.8, 135.7, 132.6, 131.6, 131.3, 130.9, 127.6, 121.1, 103.2, 100.7. HRMS (ESI): *m/z* calcd for $C_{14}H_{10}^{79}BrN_2O_4$ [M + H]$^+$: 348.9819, found 348.9822. HPLC analysis: t_R = 9.626 min, 98.2%.

4.1.28. 5,6,7-Trihydroxy-2-(2-(trifluoromethyl)phenyl)quinazolin-4(3H)-one (**A13**)

According to general procedure B, the product was obtained as a yellow solid (71 mg), yield 42%. ^{1}H NMR (400 MHz, DMSO-d_6) δ 12.62 (s, 1H), 11.70 (s, 1H), 10.35 (s, 1H), 8.94 (s, 1H), 7.94–7.85 (m, 1H), 7.84–7.69 (m, 3H), 6.57 (s, 1H). ^{13}C NMR (150 MHz, DMSO-d_6) δ 165.5, 153.9, 149.3, 147.0, 141.6, 132.9, 132.4, 131.3, 130.8, 130.4, 127.09 (q, J = 30.8 Hz), 126.41 (q, J = 4.7 Hz), 123.76 (q, J = 273 Hz), 103.0, 100.6. HRMS (ESI): *m/z* calcd for $C_{15}H_8F_3N_2O_4$ [M − H] $^-$: 337.0442, found 337.0431. HPLC analysis: t_R = 7.223 min, 96.4%.

4.1.29. 5,6,7-Trihydroxy-2-(2-(trifluoromethoxy)phenyl)quinazolin-4(3H)-one (**A15**)

According to general procedure B, the product was obtained as a white solid (71 mg), yield 40%. ^{1}H NMR (400 MHz, DMSO-d_6) δ 12.58 (s, 1H), 11.70 (s, 1H), 10.36 (s, 1H), 8.97 (s, 1H), 7.76 (dd, J = 7.6, 1.8 Hz, 1H), 7.68 (td, J = 7.8, 1.8 Hz, 1H), 7.58–7.50 (m, 2H), 6.62 (s, 1H). ^{13}C NMR (125 MHz, DMSO-d_6) δ 165.6, 153.9, 147.2, 146.7, 145.7, 141.9, 132.1, 131.4, 128.0, 127.6, 121.5, 120.0 (q, J = 257.4 Hz), 103.3, 100.5. HRMS (ESI): *m/z* calcd for $C_{15}H_8F_3N_2O_5$ [M − H] $^-$: 353.0391, found 353.0377. HPLC analysis: t_R = 9.658 min, 95.0%.

4.1.30. 5,6,7-Trihydroxy-2-(2-nitrophenyl)quinazolin-4(3H)-one (**A17**)

According to general procedure B, the product was obtained as an orange solid (68 mg), yield 43%. ^{1}H NMR (400 MHz, DMSO-d_6) δ 12.76 (s, 1H), 11.68 (s, 1H), 10.37 (s, 1H), 8.97 (s, 1H), 8.20–8.16 (m, 1H), 7.94–7.76 (m, 3H), 6.54 (s, 1H). ^{13}C NMR (125 MHz, DMSO-d_6) δ 165.7, 153.9, 148.4, 147.6, 146.8, 141.9, 133.8, 131.6, 131.5, 131.4, 129.0, 124.5, 103.2, 100.6. HRMS (ESI): *m/z* calcd for $C_{14}H_8N_3O_6$ [M − H] $^-$: 314.0419, found 314.0411. HPLC analysis: t_R = 6.699 min, 95.1%.

4.1.31. 5,6,7-Trihydroxy-2-(3-isopropylphenyl)quinazolin-4(3H)-one (**A20**)

According to general procedure B, the product was obtained as a white solid (72 mg), yield 46%. ^{1}H NMR (400 MHz, DMSO-d_6) δ 12.46 (s, 1H), 11.83 (s, 1H), 10.30 (s, 1H), 8.87 (s, 1H), 7.98 (s, 1H), 7.94–7.89 (m, 1H), 7.44 (d, J = 4.8 Hz, 2H), 6.64 (s, 1H), 2.99 (hept, J = 6.8 Hz, 1H), 1.27 (s, 3H), 1.26 (s, 3H). ^{13}C NMR (150 MHz, DMSO-d_6) δ 166.6, 153.9, 150.0, 148.8, 146.8, 141.8, 132.6, 131.0, 129.2, 128.6, 125.4, 125.2, 102.8, 100.5, 33.5, 23.8. HRMS (ESI): *m/z* calcd for $C_{17}H_{15}N_2O_4$ [M − H] $^-$: 311.1037, found 311.1033. HPLC analysis: t_R = 13.162 min, 97.7%.

4.1.32. 5,6,7-Trihydroxy-2-(thiophen-2-yl)quinazolin-4(3H)-one (**B1**)

According to general procedure B, the product was obtained as a offwhite solid (83 mg), yield 60%. ^{1}H NMR (400 MHz, DMSO-d_6) δ 12.59 (br, 1H), 11.75 (s, 1H), 10.33 (s, 1H), 8.90 (br, 1H), 8.16–8.11 (m, 1H), 7.85–7.78 (m, 1H), 7.24–7.17 (m, 1H), 6.54 (s, 1H). ^{13}C NMR (125 MHz, DMSO-d_6) δ 166.3, 154.0, 147.00, 145.40, 141.5, 137.5, 131.5, 131.0, 128.7, 128.5, 102.4, 100.4. HRMS (ESI): *m/z* calcd for $C_{12}H_7N_2O_4S$ [M − H] $^-$: 275.0123, found 275.0132. HPLC analysis: t_R = 7.024 min, 96.7%.

4.1.33. 5,6,7-Trihydroxy-2-(pyridin-2-yl)quinazolin-4(3H)-one (**B2**)

According to general procedure B, the product was obtained as an orange solid (61 mg), yield 45%. ^{1}H NMR (400 MHz, DMSO-d_6) δ 11.92

(s, 1H), 10.45 (s, 1H), 9.04 (s, 1H), 8.73 (d, $J = 4.6$ Hz, 1H), 8.36 (d, $J = 7.8$ Hz, 1H), 8.04 (t, $J = 7.8$ Hz, 1H), 7.62 (t, $J = 6.1$ Hz, 1H), 6.74 (s, 1H). ^{13}C NMR (150 MHz, DMSO-d_6) δ 166.1, 153.8, 148.9, 148.8, 148.0, 147.0, 140.7, 137.9, 131.6, 126.3, 122.0, 102.8, 101.3. HRMS (ESI): *m/z* calcd for $C_{13}H_8N_3O_4$ [M − H] $^-$: 270.0520, found 270.0520. HPLC analysis: $t_R = 5.840$ min, 95.0%.

4.1.34. 5,6,7-Trihydroxy-2-(pyridin-4-yl)quinazolin-4(3H)-one (**B3**)

According to general procedure B, the product was obtained as an yellow solid (68 mg), yield 50%. ^{1}H NMR (400 MHz, DMSO-d_6) δ 12.68 (s, 1H), 11.73 (s, 1H), 10.44 (s, 1H), 9.07 (s, 1H), 8.82–8.73 (m, 2H), 8.12–8.05 (m, 2H), 6.70 (s, 1H). ^{13}C NMR (125 MHz, DMSO-d_6) δ 165.9, 153.9, 149.9, 149.8, 147.5, 146.7, 146.0, 141.3, 140.2, 131.8, 121.5, 103.6, 101.0. HRMS (ESI): *m/z* calcd for $C_{13}H_8N_3O_4$ [M − H] $^-$: 270.0520, found 270.0519. HPLC analysis: $t_R = 5.971$ min, 96.7%.

4.1.35. 2-(1,3-Dimethyl-1H-pyrazol-5-yl)-5,6,7-trihydroxyquinazolin-4(3H)-one (**B4**)

According to general procedure B, the product was obtained as a yellow solid (75 mg), yield 52%. ^{1}H NMR (400 MHz, DMSO-d_6) δ 12.34 (br, 1H), 11.73 (s, 1H), 10.38 (s, 1H), 8.97 (br, 1H), 6.89 (s, 1H), 6.62 (s, 1H), 4.10 (s, 3H), 2.18 (s, 3H). ^{13}C NMR (125 MHz, DMSO-d_6) δ 166.2, 153.9, 146.9, 145.7, 142.4, 141.1, 134.7, 131.4, 107.8, 103.0, 100.4, 39.6, 13.2. HRMS (ESI): *m/z* calcd for $C_{13}H_{11}N_4O_4$ [M − H] $^-$: 287.0786, found 287.0777. HPLC analysis: $t_R = 7.618$ min, 96.5%.

4.1.36. 5,6,7-Trihydroxy-2-(naphthalen-2-yl)quinazolin-4(3H)-one (**B5**)

According to general procedure B, the product was obtained as a white solid (99 mg), yield 62%. ^{1}H NMR (400 MHz, DMSO-d_6) δ 11.84 (s, 1H), 10.37 (s, 1H), 8.73 (s, 1H), 8.23 (dd, $J = 8.6$, 1.9 Hz, 1H), 8.08–7.97 (m, 3H), 7.67–7.56 (m, 2H), 6.70 (s, 1H). ^{13}C NMR (125 MHz, DMSO-d_6) δ 166.6, 154.0, 150.0, 146.9, 141.2, 134.0, 132.3, 131.3, 129.7, 128.9, 128.2, 127.9, 127.8, 127.7, 127.0, 124.4, 102.5, 100.6. HRMS (ESI): *m/z* calcd for $C_{18}H_{11}N_2O_4$ [M − H] $^-$: 319.0724, found 319.0721. HPLC analysis: $t_R = 8.708$ min, 97.4%.

4.1.37. 2-Cyclopropyl-5,6,7-trihydroxyquinazolin-4(3H)-one (**B6**)

According to general procedure B, the product was obtained as a white solid (49 mg), yield 42%. ^{1}H NMR (400 MHz, DMSO-d_6) δ 12.34 (s, 1H), 11.71 (s, 1H), 10.15 (s, 1H), 8.65 (s, 1H), 6.35 (s, 1H), 1.92–1.84 (m, 1H), 1.06–0.93 (m, 4H). ^{13}C NMR (150 MHz, DMSO-d_6) δ 166.0, 156.3, 153.8, 146.9, 141.8, 129.8, 102.0, 100.2, 13.4, 9.2. HRMS (ESI): *m/z* calcd for $C_{11}H_9N_2O_4$ [M − H] $^-$: 233.0568, found 233.0560. HPLC analysis: $t_R = 5.988$ min, 95.3%.

4.1.38. 2-Cyclopentyl-5,6,7-trihydroxyquinazolin-4(3H)-one (**B7**)

According to general procedure B, the product was obtained as a white solid (49 mg), yield 48%. ^{1}H NMR (400 MHz, DMSO-d_6) δ 12.06 (s, 1H), 11.75 (s, 1H), 10.19 (s, 1H), 8.71 (s, 1H), 6.46 (s, 1H), 3.00–2.90 (m, 1H), 1.99–1.89 (m, 2H), 1.88–1.77 (m, 2H), 1.76–1.65 (m, 2H), 1.63–1.52 (m, 2H). ^{13}C NMR (150 MHz, DMSO-d_6) δ 165.9, 157.4, 153.7, 146.8, 142.2, 130.2, 102.6, 100.4, 43.7, 30.8, 25.3. HRMS (ESI): *m/z* calcd for $C_{13}H_{13}N_2O_4$ [M − H] $^-$: 261.0881, found 261.0875. HPLC analysis: $t_R = 8.081$min, 95.7%.

4.1.39. 2-Cyclohexyl-5,6,7-trihydroxyquinazolin-4(3H)-one (**B8**)

According to general procedure B, the product was obtained as a white solid (49 mg), yield 53%. ^{1}H NMR (400 MHz, DMSO-d_6) δ 12.01 (s, 1H), 11.75 (s, 1H), 10.19 (s, 1H), 8.71 (s, 1H), 6.47 (s, 1H), 2.53–2.45 (m, 1H), 1.91–1.82 (m, 2H), 1.80–1.72 (m, 2H), 1.66 (d, $J = 10.6$ Hz, 1H), 1.58–1.45 (m, 2H), 1.35–1.13 (m, 3H). ^{13}C NMR (125 MHz, DMSO-d_6) δ 165.8, 157.6, 153.7, 146.8, 142.3, 130.3, 102.1, 100.4, 42.6, 30.2, 25.5, 25.3. HRMS (ESI): *m/z* calcd for $C_{14}H_{15}N_2O_4$ [M − H] $^-$: 275.1037, found 275.1034. HPLC analysis: $t_R = 9.657$ min, 96.3%.

4.1.40. 5,6,7-Trihydroxy-2-isopropylquinazolin-4(3H)-one (**B9**)

According to general procedure B, the product was obtained as a white solid (71 mg), yield 60%. ^{1}H NMR (400 MHz, DMSO-d_6) δ 12.03 (s, 1H), 11.73 (s, 1H), 10.16 (s, 1H), 8.69 (s, 1H), 6.48 (s, 1H), 2.81 (hept, $J = 6.8$ Hz, 1H), 1.21 (d, $J = 6.9$ Hz, 6H). ^{13}C NMR (125 MHz, DMSO-d_6) δ 166.1, 158.7, 153.7, 146.9, 142.0, 130.3, 102.4, 100.4, 33.1, 20.4. HRMS (ESI): *m/z* calcd for $C_{11}H_{11}N_2O_4$ [M − H] $^-$: 235. 0724, found 235.0721. HPLC analysis: $t_R = 5.456$ min, 96.1%.

4.1.41. 2-(tert-Butyl)-5,6,7-trihydroxyquinazolin-4(3H)-one (**B10**)

According to general procedure B, the product was obtained as a white solid (70 mg), yield 56%. ^{1}H NMR (400 MHz, DMSO-d_6) δ 11.79 (s, 1H), 10.22 (s, 1H), 8.75 (s, 1H), 6.51 (s, 1H), 1.29 (s, 9H). ^{13}C NMR (125 MHz, DMSO-d_6) δ 166.5, 160.1, 153.8, 146.7, 141.4, 130.5, 102.5, 100.1, 37.1, 27.8. HRMS (ESI): *m/z* calcd for $C_{12}H_{13}N_2O_4$ [M − H] $^-$: 249.0881, found 249.0873. HPLC analysis: $t_R = 7.203$ min, 95.2%.

4.1.42. 5,6,7-Trihydroxy-2-isobutylquinazolin-4(3H)-one (**B11**)

According to general procedure B, the product was obtained as a white solid (58 mg), yield 56%. ^{1}H NMR (400 MHz, DMSO-d_6) δ 12.08 (s, 1H), 11.70 (s, 1H), 10.21 (s, 1H), 8.74 (s, 1H), 6.48 (s, 1H), 2.39 (d, $J = 7.3$ Hz, 2H), 2.11 (hept, $J = 6.7$ Hz, 1H), 0.90 (d, $J = 6.6$ Hz, 6H). ^{13}C NMR (125 MHz, DMSO-d_6) δ 166.1, 153.7, 146.8, 142.1, 130.3, 102.4, 100.4, 43.1, 27.0, 22.1. HRMS (ESI): *m/z* calcd for $C_{12}H_{13}N_2O_4$ [M − H] $^-$: 249.0881, found 249.0879. HPLC analysis: $t_R = 9.580$ min, 98.8%.

4.1.43. 5,6,7-Trihydroxy-2-neopentylquinazolin-4(3H)-one (**B12**)

According to general procedure B, the product was obtained as a white solid (79 mg), yield 60%. ^{1}H NMR (400 MHz, DMSO-d_6) δ 11.99 (s, 1H), 11.71 (s, 1H), 10.21 (s, 1H), 8.74 (s, 1H), 6.49 (s, 1H), 2.41 (s, 2H), 0.97 (s, 9H). ^{13}C NMR (125 MHz, DMSO-d_6) δ 165.7, 153.7, 152.4, 146.8, 142.1, 130.3, 102.2, 100.1, 47.0, 31.9, 29.4. HRMS (ESI): *m/z* calcd for $C_{13}H_{15}N_2O_4$ [M − H] $^-$: 263.1037, found 263.1030. HPLC analysis: $t_R = 7.704$ min, 95.1%.

4.1.44. (E)-5,6,7-Trihydroxy-2-styrylquinazolin-4(3H)-one (**B13**)

According to general procedure B, the product was obtained as a white solid (93 mg), yield 63%. ^{1}H NMR (400 MHz, DMSO-d_6) δ 12.27 (s, 1H), 11.78 (s, 1H), 10.28 (s, 1H), 8.89 (s, 1H), 7.84 (d, $J = 16.2$ Hz, 1H), 7.69–7.60 (m, 2H), 7.51–7.37 (m, 3H), 6.93 (d, $J = 16.2$ Hz, 1H), 6.58 (s, 1H). ^{13}C NMR (125 MHz, DMSO-d_6) δ 165.6, 153.8, 148.4, 146.8, 142.1, 137.2, 135.1, 130.9, 129.5, 129.0, 127.5, 121.0, 102.8, 100.6. HRMS (ESI): *m/z* calcd for $C_{16}H_{11}N_2O_4$ [M − H] $^-$: 295.0724, found 295.0720. HPLC analysis: $t_R = 9.694$ min, 95.3%.

4.1.45. 2-Benzyl-5,6,7-trihydroxyquinazolin-4(3H)-one (**B14**)

According to general procedure B, the product was obtained as a white solid (85 mg), yield 60%. ^{1}H NMR (400 MHz, DMSO-d_6) δ 12.34 (s, 1H), 11.68 (s, 1H), 10.23 (s, 1H), 8.77 (s, 1H), 7.38–7.28 (m, 4H), 7.27–7.21 (m, 1H), 6.48 (s, 1H), 3.86 (s, 2H). ^{13}C NMR (150 MHz, DMSO-d_6) δ 166.1, 153.9, 153.6, 146.8, 141.1, 136.4, 130.7, 128.8, 128.5, 126.9, 101.6, 100.2, 40.3. HRMS (ESI): *m/z* calcd for $C_{15}H_{11}N_2O_4$ [M − H] $^-$: 283.0724, found 283.0716. HPLC analysis: $t_R = 8.088$ min, 95.0%.

4.1.46. 5,6,7-Trihydroxy-2-(1-phenylethyl)quinazolin-4(3H)-one (**B15**)

According to general procedure B, the product was obtained as a white solid (85 mg), yield 57%. ^{1}H NMR (400 MHz, DMSO-d_6) δ 12.16 (s, 1H), 11.65 (s, 1H), 10.25 (s, 1H), 8.76 (s, 1H), 7.40–7.27 (m, 4H), 7.26–7.18 (m, 1H), 6.54 (s, 1H), 4.03 (q, $J = 7.0$ Hz, 1H), 1.55 (d, $J = 7.0$ Hz, 3H). ^{13}C NMR (125 MHz, DMSO-d_6) δ 165.8, 155.9, 153.8, 146.8, 142.4, 142.0, 130.5, 128.5, 127.4, 126.8, 102.8, 100.4, 43.6, 19.3. HRMS (ESI): *m/z* calcd for $C_{16}H_{13}N_2O_4$ [M − H] $^-$: 297. 0881, found 297. 0871. HPLC analysis: $t_R = 7.318$ min, 97.7%.

4.1.47. 5,6,7-Trihydroxy-2-(1-phenylpropyl)quinazolin-4(3H)-one (**B16**)

According to general procedure B, the product was obtained as a white solid (92 mg), yield 59%. ^{1}H NMR (400 MHz, DMSO-d_6) δ 11.69 (br, 1H), 10.27 (br, 1H), 7.42–7.35 (m, 2H), 7.34–7.29 (m, 2H), 7.26–7.20 (m, 1H), 6.55 (s, 1H), 3.74 (t, J = 7.7 Hz, 1H), 2.27–2.15 (m, 1H), 1.96–1.84 (m, 1H), 0.83 (t, J = 7.3 Hz, 3H). ^{13}C NMR (125 MHz, DMSO-d_6) δ 166.1, 156.2, 154.5, 153.9, 146.8, 140.7, 130.7, 128.5, 127.9, 127.1, 101.8100.4, 51.2, 26.3, 12.2. HRMS (ESI): *m/z* calcd for $C_{17}H_{15}N_2O_4$ [M − H] $^-$: 311.1037, found 311.1028. HPLC analysis: t_R = 7.867 min, 95.1%.

4.1.48. 5,6,7-Trihydroxy-2-(2-methyl-1-phenylpropyl)quinazolin-4(3H)-one (**B17**)

According to general procedure B, the product was obtained as a white solid (103 mg), yield 63%. ^{1}H NMR (400 MHz, DMSO-d_6) δ 12.23 (s, 1H), 11.61 (s, 1H), 10.24 (s, 1H), 8.76 (s, 1H), 7.44 (d, J = 7.1 Hz, 2H), 7.31 (t, J = 7.5 Hz, 2H), 7.25–7.18 (m, 1H), 6.55 (s, 1H), 3.40 (d, J = 11.3 Hz, 1H), 2.67–2.53 (m, 1H), 0.93 (d, J = 6.4 Hz, 3H), 0.69 (d, J = 6.6 Hz, 3H). ^{13}C NMR (125 MHz, DMSO-d_6) δ 165.7, 155.4, 153.8, 146.7, 142.3, 140.3, 130.4, 128.33, 128.28, 127.0, 102.7, 100.2, 57.8, 30.9, 21.2, 20.5. HRMS (ESI): *m/z* calcd for $C_{18}H_{18}N_2O_4Na$ [M + Na]$^+$: 349. 1159, found 349. 1158. HPLC analysis: t_R = 9.494 min, 96.0%.

4.1.49. 5,6,7-Trihydroxy-3-isobutyl-2-phenylquinazolin-4(3H)-one (**C1**)

According to general procedure B, the product was obtained as a light yellow solid (77 mg), yield 47%. ^{1}H NMR (400 MHz, DMSO-d_6) δ 11.83 (s, 1H), 10.37 (s, 1H), 8.95 (s, 1H), 7.61–7.56 (m, 2H), 7.55–7.47 (m, 3H), 6.57 (s, 1H), 3.83 (d, J = 7.4 Hz, 2H), 1.73 (hept, J = 6.9 Hz, 1H), 0.61 (d, J = 6.7 Hz, 6H). ^{13}C NMR (125 MHz, DMSO-d_6) δ 165.2, 153.9, 153.0, 146.4, 140.3, 135.2, 131.4, 129.5, 128.5, 128.3, 102.8, 100.4, 50.6, 27.3, 19.7. HRMS (ESI): *m/z* calcd for $C_{18}H_{19}N_2O_4$ [M + H] $^+$: 327.1339, found 327.1342. HPLC analysis: t_R = 14.369 min, 96.7%.

4.1.50. 5,6,7-Trihydroxy-3-(2-hydroxyethyl)-2-phenylquinazolin-4(3H)-one (**C2**)

According to general procedure B, the product was obtained as a white solid (71 mg), yield 45%. ^{1}H NMR (400 MHz, DMSO-d_6) δ 11.80 (s, 1H), 10.33 (s, 1H), 8.93 (s, 1H), 7.62–7.55 (m, 2H), 7.54–7.47 (m, 3H), 6.55 (s, 1H), 4.83 (t, J = 5.7 Hz, 1H), 3.94 (t, J = 6.2 Hz, 2H), 3.48 (q, J = 5.9 Hz, 2H). ^{13}C NMR (125 MHz, DMSO-d_6) δ 165.1, 153.9, 153.4, 146.4, 140.5, 135.4, 131.3, 129.3, 128.6, 128.3, 102.6, 100.7, 57.8, 46.9. HRMS (ESI): *m/z* calcd for $C_{16}H_{15}N_2O_5$ [M + H] $^+$: 315. 0976, found 315. 0973. HPLC analysis: t_R = 11.691 min, 98.1%.

4.1.51. N-(tert-butyl)-2-(5,6,7-trihydroxy-4-oxo-2-phenylquinazolin-3(4H)-yl)acetamide (**C3**)

According to general procedure B, the product was obtained as a white solid (82 mg), yield 43%. ^{1}H NMR (400 MHz, DMSO-d_6) δ 11.57 (s, 1H), 10.39 (s, 1H), 8.96 (br, 1H), 7.67 (s, 1H), 7.58–7.43 (m, 5H), 6.58 (s, 1H), 4.36 (s, 2H), 1.17 (s, 9H). ^{13}C NMR (125 MHz, DMSO-d_6) δ 165.4, 164.7, 154.0, 153.1, 146.3, 140.4, 134.8, 131.4, 129.6, 128.3, 128.1, 102.8, 100.2, 50.3, 47.1, 28.3. HRMS (ESI): *m/z* calcd for $C_{20}H_{21}N_3O_5Na$ [M + Na] $^+$: 406. 1373, found 406.1370. HPLC analysis: t_R = 12.294 min, 96.8%.

4.1.52. 3-Cyclopropyl-5,6,7-trihydroxy-2-phenylquinazolin-4(3H)-one (**C4**)

According to general procedure B, the product was obtained as a white solid (71 mg), yield 46%.^{1}H NMR (400 MHz, DMSO-d_6) δ 11.88 (s, 1H), 10.26 (s, 1H), 8.88 (s, 1H), 7.84–7.66 (m, 2H), 7.56–7.41 (m, 3H), 6.55 (s, 1H), 3.17 (tt, J = 7.3, 4.1 Hz, 1H), 0.87–0.65 (m, 2H), 0.57–0.30 (m, 2H). ^{13}C NMR (125 MHz, DMSO-d_6) δ 166.7, 153.9, 153.6, 146.4, 140.1, 136.0, 131.2, 129.3, 128.4, 127.9, 102.7, 100.4, 29.0, 10.7. HRMS (ESI): *m/z* calcd for $C_{17}H_{15}N_2O_4$ [M + H] $^+$: 311. 1026, found 311. 1023. HPLC analysis: t_R = 12.671 min, 98.4%.

4.1.53. 3-Cyclopentyl-5,6,7-trihydroxy-2-phenylquinazolin-4(3H)-one (**C5**)

According to general procedure B, the product was obtained as a white solid (85 mg), yield 50%. ^{1}H NMR (400 MHz, DMSO-d_6) δ 11.90 (s, 1H), 10.30 (s, 1H), 8.91 (s, 1H), 7.70–7.38 (m, 5H), 6.53 (s, 1H), 4.35–4.25 (m, 1H), 2.34–2.21 (m, 2H), 1.96–1.82 (m, 2H), 1.79–1.65 (m, 2H), 1.46–1.34 (m, 2H). ^{13}C NMR (125 MHz, DMSO-d_6) δ 165.4, 153.8, 153.7, 146.5, 140.1, 135.9, 131.3, 129.5, 128.6, 127.8, 102.4, 101.4, 61.0, 28.7, 25.4. HRMS (ESI): *m/z* calcd for $C_{19}H_{19}N_2O_4$ [M + H] $^+$: 339.1339, found 339.1338. HPLC analysis: t_R = 11.188 min, 96.5%.

4.1.54. 3-Cyclohexyl-5,6,7-trihydroxy-2-phenylquinazolin-4(3H)-one (**C6**)

According to general procedure B, the product was obtained as a white solid (97 mg), yield 55%. ^{1}H NMR (400 MHz, DMSO-d_6) δ 11.98 (s, 1H), 10.30 (s, 1H), 8.91 (s, 1H), 7.60–7.48 (m, 5H), 6.52 (s, 1H), 3.71 (t, J = 12.1 Hz, 1H), 2.58–2.43 (m, 2H), 1.81–1.62 (m, 4H), 1.54–1.42 (m, 1H), 1.16–0.98 (m, 1H), 0.91–0.73 (m, 2H). ^{13}C NMR (125 MHz, DMSO-d_6) δ 166.4, 154.2, 153.9, 147.0, 140.5, 136.4, 131.7, 129.9, 129.0, 127.9, 102.9, 101.9, 62.0, 28.8, 26.3, 25.1. HRMS (ESI): *m/z* calcd for $C_{20}H_{21}N_2O_4$ [M + H] $^+$: 353.1496, found 353.1503. HPLC analysis: t_R = 8.000 min, 98.4%.

4.1.55. 5,6,7-Trihydroxy-2,3-diphenylquinazolin-4(3H)-one (**C7**)

According to general procedure B, the product was obtained as a white solid (99 mg), yield 57%. ^{1}H NMR (400 MHz, DMSO-d_6) δ 11.60 (s, 1H), 10.42 (s, 1H), 9.00 (s, 1H), 7.37–7.15 (m, 10H), 6.67 (s, 1H). ^{13}C NMR (125 MHz, DMSO-d_6) δ 165.0, 154.1, 152.1, 146.8, 140.7, 136.9, 135.3, 131.5, 129.6, 129.0, 128.8, 128.6, 128.3, 127.5, 103.2, 100.4. HRMS (ESI): *m/z* calcd for $C_{20}H_{15}N_2O_4$ [M + H] $^+$: 347.1026, found 347.1025. HPLC analysis: t_R = 8.939 min, 98.9%.

4.1.56. 3-(2-Fluorophenyl)-5,6,7-trihydroxy-2-phenylquinazolin-4(3H)-one (**C8**)

According to general procedure B, the product was obtained as a white solid (73 mg), yield 40%. ^{1}H NMR (400 MHz, DMSO-d_6) δ 11.32 (s, 1H), 10.50 (s, 1H), 9.07 (s, 1H), 7.51 (td, J = 7.8, 1.7 Hz, 1H), 7.43–7.20 (m, 7H), 7.16 (td, J = 7.7, 1.4 Hz, 1H), 6.70 (s, 1H). ^{13}C NMR (125 MHz, DMSO-d_6) δ 164.3, 157.0 (d, J = 248.1 Hz), 154.3, 151.7, 146.8, 140.4, 134.5, 131.7 (d, J = 24.6 Hz) 131.2 (d, J = 8.2 Hz), 129.3, 128.3, 127.7, 124.7 (d, J = 3.4 Hz), 124.5, 124.4, 115.8 (d, J = 19.6 Hz), 103.6, 99.9. HRMS (ESI): *m/z* calcd for $C_{20}H_{14}FN_2O_4$ [M + H] $^+$: 365.0932, found 365.0931. HPLC analysis: t_R = 7.934 min, 98.3%.

4.1.57. 3-(3-Fluorophenyl)-5,6,7-trihydroxy-2-phenylquinazolin-4(3H)-one (**C9**)

According to general procedure B, the product was obtained as a white solid (73 mg), yield 40%. ^{1}H NMR (400 MHz, DMSO-d_6) δ 11.50 (s, 1H), 10.44 (s, 1H), 9.03 (s, 1H), 7.45–7.07 (m, 9H), 6.67 (s, 1H). ^{13}C NMR (125 MHz, DMSO-d_6) δ 164.8, 161.6 (d, J = 244.4 Hz), 154.1, 151.8, 146.8, 140.5, 138.4 (d, J = 10.6 Hz), 135.1, 131.6, 130.1 (d, J = 9.0 Hz), 128.9, 127.6, 126.1 (d, J = 3.1 Hz), 117.2 (d, J = 23.7 Hz), 115.4 (d, J = 20.8 Hz), 103.3, 100.3. HRMS (ESI): *m/z* calcd for $C_{20}H_{14}FN_2O_4$ [M + H] $^+$: 365.0932, found 365.0930. HPLC analysis: t_R = 7.986 min, 96.7%.

4.1.58. 5,6,7-Trihydroxy-3-(4-hydroxyphenyl)-2-phenylquinazolin-4(3H)-one (**C10**)

According to general procedure B, the product was obtained as a white solid (94 mg), yield 52%. ^{1}H NMR (400 MHz, DMSO-d_6) δ 11.69 (s, 1H), 10.37 (s, 1H), 9.62 (s, 1H), 8.97 (s, 1H), 7.34–7.29 (m, 2H), 7.27–7.19 (m, 3H), 7.10–7.05 (m, 2H), 6.65–6.60 (m, 3H). ^{13}C NMR (125 MHz, DMSO-d_6) δ 165.3, 157.0, 154.0, 152.6, 146.8, 140.7, 135.6, 131.4, 130.5, 129.0, 128.7, 127.9, 127.5, 115.1, 103.1, 100.5. HRMS (ESI): *m/z* calcd for $C_{20}H_{15}N_2O_5$ [M + H] $^+$: 363.0976, found 363.0984. HPLC analysis: t_R = 7.195 min, 98.2%.

*4.1.59. 3-(4-Bromo-2-fluorophenyl)-5,6,7-trihydroxy-2-phenylquinazolin-4(3H)-one(**C11**)*

According to general procedure B, the product was obtained as a white solid (93 mg), yield 42%. ^{1}H NMR (400 MHz, DMSO-d_6) δ 11.23 (s, 1H), 10.57 (s, 1H), 9.13 (br, 1H), 7.66 (dd, J = 9.4, 2.1 Hz, 1H), 7.53 (t, J = 8.2 Hz, 1H), 7.42 (dd, J = 8.6, 2.1 Hz, 1H), 7.39–7.25 (m, 5H), 6.70 (s, 1H). ^{13}C NMR (125 MHz, DMSO-d_6) δ 164.1, 156.9 (d, J = 253.0 Hz), 154.4, 151.4, 146.8, 140.3, 134.3, 133.2, 131.9, 129.5, 128.3, 128.0 (d, J = 3.4 Hz), 127.9, 124.2 (d, J = 13.1 Hz), 122.7 (d, J = 9.0 Hz), 119.4 (d, J = 23.2 Hz), 103.7, 99.8. HRMS (ESI): m/z calcd for $C_{20}H_{11}^{79}BrFN_2O_4$ [M − H]$^-$: 440.9892, found 440.9878. HPLC analysis: t_R = 8.670 min, 97.1%.

*4.1.60. 3-(4-Fluoro-3-methylphenyl)-5,6,7-trihydroxy-2-phenylquinazolin-4(3H)-one (**C12**)*

According to general procedure B, the product was obtained as a white solid (108 mg), yield 57%. ^{1}H NMR (400 MHz, DMSO-d_6) δ 11.57 (s, 1H), 10.42 (br, 1H), 9.01 (br, 1H), 7.38–7.29 (m, 3H), 7.31–7.13 (m, 4H), 7.06 (t, J = 9.1 Hz, 1H), 6.66 (s, 1H), 2.12 (d, J = 1.9 Hz, 3H). ^{13}C NMR (125 MHz, DMSO-d_6) δ 165.0, 159.8 (d, J = 244.8 Hz), 154.1, 152.0, 146.8, 140.5, 135.2, 132.69 (d, J = 3.4 Hz), 132.66, 132.61, 131.5, 128.9, 128.8 (d, J = 9.2 Hz), 127.5, 124.5 (d, J = 18.8 Hz), 115.0 (d, J = 23.7 Hz), 103.2, 100.3, 14.0 (d, J = 3.1 Hz). HRMS (ESI): m/z calcd for $C_{21}H_{16}FN_2O_4$ [M + H] $^+$: 379. 1089, found 379.1089. HPLC analysis: t_R = 8.177 min, 96.6%.

*4.1.61. 3-([1,1′-biphenyl]-4-yl)-5,6,7-trihydroxy-2-phenylquinazolin-4 (3H)-one (**C13**)*

According to general procedure B, the product was obtained as a white solid (74 mg), yield 35%. ^{1}H NMR (400 MHz, DMSO-d_6) δ 11.61 (s, 1H), 10.44 (s, 1H), 9.02 (s, 1H), 7.67–7.60 (m, 4H), 7.50–7.33 (m, 7H), 7.28–7.19 (m, 3H), 6.68 (s, 1H). ^{13}C NMR (125 MHz, DMSO-d_6) δ 165.1, 154.1, 152.0, 146.8, 140.7, 139.7, 138.8, 136.2, 135.3, 131.6, 130.1, 129.1, 129.0, 128.9, 127.8, 127.6, 126.7, 126.7, 126.6, 103.3, 100.4. HRMS (ESI): m/z calcd for $C_{26}H_{19}N_2O_4$ [M + H] $^+$: 423. 1340, found 423. 1345. HPLC analysis: t_R = 10.271 min, 97.1%.

*4.1.62. 5,6,7-Trihydroxy-2-phenyl-3-(pyridin-3-yl)quinazolin-4(3H)-one (**C14**)*

According to general procedure B, the product was obtained as a white solid (74 mg), yield 50%. ^{1}H NMR (400 MHz, DMSO-d_6) δ 11.42 (s, 1H), 10.49 (s, 1H), 9.06 (s, 1H), 8.52 (d, J = 2.4 Hz, 1H), 8.43 (dd, J = 4.8, 1.5 Hz, 1H), 7.88–7.83 (m, 1H), 7.44–7.30 (m, 3H), 7.29–7.19 (m, 3H), 6.69 (s, 1H). ^{13}C NMR (125 MHz, DMSO-d_6) δ 164.9, 154.2, 151.7, 150.0, 149.0, 146.8, 140.6, 137.2, 134.9, 133.9, 131.7, 129.1, 129.0, 127.7, 123.5, 103.4, 100.2. HRMS (ESI): m/z calcd for $C_{19}H_{14}N_3O_4$ [M + H] $^+$: 348.0979, found 348.0974. HPLC analysis: t_R = 6.881min, 97.9%.

*4.1.63. 5,6,7-Trihydroxy-2-phenyl-3-(1H-pyrazol-4-yl)quinazolin-4(3H)-one (**C15**)*

According to general procedure B, the product was obtained as a white solid (82 mg), yield 49%. ^{1}H NMR (400 MHz, DMSO-d_6) δ 12.86 (br, 1H), 11.62 (s, 1H), 10.44 (s, 1H), 9.00 (s, 1H), 7.69 (br, 1H), 7.42–7.35 (m, 2H), 7.32–7.23 (m, 3H), 6.64 (s, 1H). ^{13}C NMR (125 MHz, DMSO-d_6) δ 165.1, 154.1, 152.9, 146.8, 140.4, 135.4, 131.5, 128.9, 128.9, 127.6, 117.8, 103.2, 100.2. HRMS (ESI): m/z calcd for $C_{17}H_{11}N_4O_4$ [M − H] $^-$: 335.0786, found 335.0779. HPLC analysis: t_R = 8.686 min, 95.4%.

*4.1.64. 5,6,7-Trihydroxy-2-isobutyl-3-phenylquinazolin-4(3H)-one (**D6**)*

According to general procedure B, the product was obtained as a white solid (98 mg), yield 60%. ^{1}H NMR (400 MHz, DMSO-d_6) δ 11.53 (s, 1H), 10.27 (s, 1H), 8.82 (s, 1H), 7.62–7.48 (m, 3H), 7.47–7.39 (m, 2H), 6.57 (s, 1H), 2.16 (d, J = 6.9 Hz, 2H), 2.08–1.96 (m, 1H), 0.78 (d, J = 6.6 Hz, 6H). ^{13}C NMR (125 MHz, DMSO-d_6) δ 165.1, 153.9, 152.7, 146.7, 140.6, 136.4, 130.8, 129.4, 129.0, 128.9, 102.6, 100.1, 43.2, 25.8, 22.2. HRMS (ESI): m/z calcd for $C_{18}H_{19}N_2O_4$ [M + H]$^+$: 327.1339, found 327.1345. HPLC analysis: t_R = 8.174 min, 99.8%.

*4.1.65. 3-(2-Fluorophenyl)-5,6,7-trihydroxy-2-isobutylquinazolin-4(3H)-one (**D7**)*

According to general procedure B, the product was obtained as a white solid (107 mg), yield 62%. ^{1}H NMR (400 MHz, DMSO-d_6) δ 11.26 (s, 1H), 10.43 (br, 1H), 7.71–7.58 (m, 2H), 7.54–7.46 (m, 1H), 7.42 (t, J = 7.4 Hz, 1H), 6.60 (s, 1H), 2.29–2.12 (m, 2H), 1.99 (hept, J = 6.7 Hz, 1H), 0.80 (dd, J = 8.2, 6.6 Hz, 6H). ^{13}C NMR (125 MHz, DMSO-d_6) δ 163.9, 157.3 (d, J = 248.5 Hz), 154.4, 153.1, 146.7, 145.9, 139.3, 132.0 (d, J = 7.9 Hz), 131.3 (d, J = 43.4 Hz), 125.5 (d, J = 3.6 Hz), 123.4 (d, J = 13.4 Hz), 116.5 (d, J = 19.4 Hz), 102.3, 99.6, 42.7, 25.9, 22.1 (d, J = 7.7 Hz). HRMS (ESI): m/z calcd for $C_{18}H_{17}FN_2O_4$ [M − H]$^-$: 343.1100, found 343.1090. HPLC analysis: t_R = 9.123 min, 96.3%.

*4.1.66. 3-(4-Fluoro-3-methylphenyl)-5,6,7-trihydroxy-2-isobutylquinazolin-4(3H)-one (**D8**)*

According to general procedure B, the product was obtained as a white solid (107 mg), yield 60%. ^{1}H NMR (400 MHz, DMSO-d_6) δ 11.51 (s, 1H), 10.31 (s, 1H), 8.84 (s, 1H), 7.42–7.37 (m, 1H), 7.34–7.29 (m, 2H), 6.56 (s, 1H), 2.28 (d, J = 2.1 Hz, 3H), 2.17 (d, J = 6.3 Hz, 2H), 2.11–1.98 (m, 1H), 0.81 (dd, J = 6.6, 1.9 Hz, 6H). ^{13}C NMR (125 MHz, DMSO-d_6) δ 165.1, 160.5 (d, J = 245.1 Hz), 154.0, 152.7, 146.7, 140.6, 132.2 (d, J = 3.2 Hz), 132.0 (d, J = 5.8 Hz), 130.9, 128.3 (d, J = 8.8 Hz), 125.7 (d, J = 18.7 Hz), 115.9 (d, J = 23.7 Hz), 102.6, 100.1, 43.1, 25.8, 22.3 (d, J = 5.4 Hz), 14.1 (d, J = 2.9 Hz). HRMS (ESI): m/z calcd for $C_{19}H_{18}FN_2O_4$ [M − H]$^-$: 357.1256, found 357.1252. HPLC analysis: t_R = 10.674 min, 95.2%.

*4.1.67. 3-(4-Bromo-2-fluorophenyl)-5,6,7-trihydroxy-2-isobutylquinazolin-4(3H)-one (**D9**)*

According to general procedure B, the product was obtained as a white solid (116 mg), yield 55%. ^{1}H NMR (400 MHz, DMSO-d_6) δ 11.17 (s, 1H), 10.43 (br, 1H), 7.94–7.87 (m, 1H), 7.70–7.61 (m, 2H), 6.60 (s, 1H), 2.29–2.11 (m, 2H), 2.01 (hept, J = 6.6 Hz, 1H), 0.82 (dd, J = 7.8, 6.6 Hz, 6H). ^{13}C NMR (125 MHz, DMSO-d_6) δ 164.1, 157.2 (d, J = 253.0 Hz), 154.3, 152.0, 146.7, 140.2, 132.6, 131.3, 128.8 (d, J = 3.5 Hz), 123.3, 123.2 (d, J = 5.4 Hz), 120.1(d, J = 23.2 Hz), 102.9, 99.5, 42.8, 25.7, 22.1 (d, J = 2.7 Hz). HRMS (ESI): m/z calcd for $C_{18}H_{15}^{79}BrFN_2O_4$ [M − H]$^-$: 421.0205, found 421.0200. HPLC analysis: t_R = 10.166 min, 96.6%.

4.1.68. General procedure C for the preparation of D1–D4, D10 and D11

To a solution of compound **33a or 33b** (1 mmol) in anhydrous acetonitrile (8 mL) was added the corresponding anilines (1.2 mmol) and PCl_3 (0.18 mL, 2 mmol) at 0 °C, and the resulting suspension was heated to 50 °C and stirred for 4–12 h. Then, the reaction was moved to 0 °C and was quenched by adding 1 N aqueous HCl solution. The aqueous portion was extracted with DCM (3 × 20 mL), and the combined organics were washed with 10% aqueous $NaHCO_3$ solution and brine, dried over anhydrous Na_2SO_4, filtered, and concentrated under reduced pressure. The residue was purified by silica column chromatography (petroleum ether/EtOAc = 8:1 to 6:1) to give the corresponding quinazolinones **35a**–**35f**.

According to general procedure A, the demethylation of the above quinazolinones afforded the target compounds **D1**–**D4**, **D10** and **D11**.

*4.1.69. 5,6,7-Trihydroxy-3-phenyl-2-(1-phenylethyl)quinazolin-4(3H)-one (**D1**)*

According to general procedure C, the product was obtained as a white solid (118 mg), yield 63%. ^{1}H NMR (400 MHz, DMSO-d_6) δ 11.49 (s, 1H), 10.39 (s, 1H), 8.92 (s, 1H), 7.57 (d, J = 4.5 Hz, 2H), 7.49–7.40 (m, 1H), 7.23–7.12 (m, 4H), 6.80 (dd, J = 6.6, 2.9 Hz, 2H), 6.68 (s, 1H), 6.54–6.48 (m, 1H), 3.81 (q, J = 6.8 Hz, 1H), 1.46 (d, J = 6.9 Hz, 3H). ^{13}C NMR (125 MHz, DMSO-d_6) δ 165.2, 155.0, 154.0, 146.7, 142.3, 140.3,

135.8, 131.2, 129.6, 129.4, 128.9, 128.7, 128.4, 127.1, 126.6, 103.1, 100.3, 43.2, 21.8.

HRMS (ESI): *m/z* calcd for $C_{22}H_{19}N_2O_4$ $[M + H]^+$: 375. 1339, found 375. 1345. HPLC analysis: t_R = 9.099 min, 99.1%.

*4.1.70. 3-(4-Fluoro-3-methylphenyl)-5,6,7-trihydroxy-2-(1-phenylethyl) quinazolin-4(3H)-one (**D2**)*

According to general procedure C, the product was obtained as a white solid (106 mg), yield 52%. ^{1}H NMR (400 MHz, DMSO-d_6) δ 11.46 (s, 1H), 10.40 (s, 1H), 8.92 (s, 1H), 7.54–7.48 (m, 0.4 H), 7.49–7.39 (m, 0.6 H), 7.32 (t, J = 9.0 Hz, 0.6 H), 7.23–7.11 (m, 3H), 6.94 (t, J = 9.1 Hz, 0.4H), 6.88–6.81 (m, 1H), 6.80–6.72 (m, 1H), 6.68 (d, J = 4.5 Hz, 1H), 6.36–6.28 (m, 0.4 H), 6.20–6.14 (m, 0.6H), 3.89–3.74 (m, 1H), 2.31 (s, 1.2 H), 1.91 (s, 1.9 H), 1.45 (dd, J = 6.9, 3.1 Hz, 3H). ^{13}C NMR (125 MHz, DMSO-d_6) δ 165.2, 161.6 (d, J = 5.0 Hz), 159.2 (d, J = 5.0 Hz), 154.9 (d, J = 8.7 Hz), 154.1 (d, J = 1.9 Hz), 146.7, 142.6, 142.4, 140.3 (d, J = 1.2 Hz), 133.1 (d, J = 6.0 Hz), 131.7 (d, J = 5.7 Hz), 131.5 (d, J = 3.3 Hz), 131.4 (d, J = 3.2 Hz), 131.2, 128.9 (d, J = 8.9 Hz), 128.4 (d, J = 4.7 Hz), 128.0 (d, J = 8.8 Hz), 127.1 (d, J = 6.9 Hz), 126.6 (d, J = 7.8 Hz), 125.5 (d, J = 18.7 Hz), 124.7 (d, J = 18.9 Hz), 115.7 (d, J = 23.9 Hz), 115.0 (d, J = 23.6 Hz), 103.2, 103.1, 100.2, 43.7, 43.3, 22.0, 21.9, 14.2 (d, J = 2.9 Hz), 13.8 (d, J = 3.1 Hz). HRMS (ESI): *m/z* calcd for $C_{23}H_{20}FN_2O_4$ $[M + H]^+$: 407.1402, found 407.1395. HPLC analysis: t_R = 13.337 min, 96.5%.

*4.1.71. 3-(2-Fluorophenyl)-5,6,7-trihydroxy-2-(1-phenylethyl)quinazolin-4(3H)-one (**D3**)*

According to general procedure C, the product was obtained as a white solid (110 mg), yield 56%. ^{1}H NMR (400 MHz, DMSO-d_6) δ 11.28 (s, 1H), 10.45 (s, 1H), 8.96 (s, 1H), 7.81–7.71 (m, 1H), 7.58–7.44 (m, 1H), 7.43–7.35 (m, 1H), 7.26–7.03 (m, 3H), 7.03–6.93 (m, 1H), 6.72 (s, 1H), 6.71–6.60 (m, 2H), 3.95 (q, J = 6.7 Hz, 1H), 1.47 (d, J = 6.8 Hz, 3H). ^{13}C NMR (125 MHz, DMSO-d_6) δ 164.4, 157.7 (d, J = 250.6 Hz), 154.5, 154.3, 146.7, 141.3, 140.2, 131.6 (d, J = 8.0 Hz), 131.5, 130.6, 128.5, 128.3, 126.8, 126.7, 125.0 (d, J = 3.5 Hz), 123.3 (d, J = 13.4 Hz), 116.1, 115.9, 103.4, 99.7, 43.5, 21.9. HRMS (ESI): *m/z* calcd for $C_{22}H_{18}FN_2O_4$ $[M + H]^+$: 393. 1245, found 393. 1251. HPLC analysis: t_R = 8.657 min, 96.6%.

*4.1.72. 3-(4-Bromo-2-fluorophenyl)-5,6,7-trihydroxy-2-(1-phenylethyl) quinazolin-4(3H)-one (**D4**)*

According to general procedure C, the product was obtained as a white solid (141 mg), yield 60%. ^{1}H NMR (400 MHz, DMSO-d_6) δ 11.18 (s, 1H), 10.48 (s, 1H), 8.98 (s, 1H), 7.77 (t, J = 8.2 Hz, 1H), 7.63 (dd, J = 8.5, 2.1 Hz, 1H), 7.32 (dd, J = 9.3, 2.1 Hz, 1H), 7.17–7.09 (m, 3H), 6.74–6.68 (m, 3H), 3.95 (q, J = 6.7 Hz, 1H), 1.47 (d, J = 6.8 Hz, 3H). ^{13}C NMR (125 MHz, DMSO-d_6) δ 164.1, 158.6, 156.6, 154.3, 154.1, 146.7, 141.2, 140.0, 132.1, 131.5, 128.4, 128.3 (d, J = 3.5 Hz), 126.8, 126.7, 123.1–122.9 (m), 119.3 (d, J = 23.2 Hz), 103.5, 99.6, 43.6, 21.9. HRMS (ESI): *m/z* calcd for $C_{22}H_{17}^{79}BrFN_2O_4$ $[M + H]^+$: 471.0350, found 471.0352. HPLC analysis: t_R = 13.244 min, 99.4%.

*4.1.73. 2-Benzyl-5,6,7-trihydroxy-3-phenylquinazolin-4(3H)-one (**D10**)*

According to general procedure C, the product was obtained as a white solid (112 mg), yield 62%. ^{1}H NMR (400 MHz, DMSO-d_6) δ 11.48 (s, 1H), 10.33 (s, 1H), 8.88 (s, 1H), 7.49–7.38 (m, 3H), 7.23–7.14 (m, 5H), 6.90–6.82 (m, 2H), 6.59 (s, 1H), 3.75 (s, 2H). ^{13}C NMR (125 MHz, DMSO-d_6) δ 165.1, 154.0, 152.2, 146.7, 140.5, 136.0, 135.8, 131.2, 129.1, 129.0, 128.5, 128.2, 126.6, 102.8, 100.3, 41.3. HRMS (ESI): *m/z* calcd for $C_{21}H_{17}N_2O_4$ $[M + H]^+$: 361.1183, found 361.1190. HPLC analysis: t_R = 8.737 min, 95.8%.

*4.1.74. 2-Benzyl-3-(4-fluoro-3-methylphenyl)-5,6,7-trihydroxyquinazolin-4(3H)-one (**D11**)*

According to general procedure C, the product was obtained as a white solid (88 mg), yield 45%. ^{1}H NMR (400 MHz, DMSO-d_6) δ 11.44 (s, 1H), 10.35 (s, 1H), 8.89 (s, 1H), 7.23–7.16 (m, 4H), 7.14–7.08 (m, 1H), 6.94 (dd, J = 7.0, 2.6 Hz, 1H), 6.88–6.83 (m, 2H), 6.60 (s, 1H), 3.77 (q, J = 15.5 Hz, 2H), 2.12 (d, J = 1.8 Hz, 3H). ^{13}C NMR (125 MHz, DMSO-d_6) δ 165.6, 160.9 (d, J = 245.1 Hz), 154.5, 152.8, 147.2, 140.9, 136.2, 132.8 (d, J = 5.8 Hz), 132.1 (d, J = 3.2 Hz), 131.7, 128.9, 128.7 (d, J = 9.0 Hz), 128.6, 127.0, 125.6 (d, J = 18.8 Hz), 116.0 (d, J = 23.9 Hz), 103.3, 100.7, 42.0, 14.4 (d, J = 2.9 Hz). HRMS (ESI): *m/z* calcd for $C_{25}H_{18}FN_2O_4$ $[M + H]^+$: 393.1245, found 393.1249. HPLC analysis: t_R = 12.068 min, 96.2%.

4.1.75. General procedure D for the preparation of D5 and D12

To the stirred solution of the prepared 2-phenylpropanoyl chloride or commercially available phenylacetyl chloride (1 mmol) in pyridine (5 mL) was added TPP (816 mg, 2.5 mmol) under the N_2 atmosphere at 0 °C, and the reaction mixture was heated to 70 °C and stirred for 2 h. Then the reaction mixture was cooled to room temperature, and was treated with isobutylamine (**40**) (0.12 mL, 1.2 mmol). Then the resulting mixture was heated to 70 °C and stirred overnight. After completion, the reaction mixture was cooled to room temperature, and the solvent was removed under reduced pressure to obtain the residue. The residue was then diluted with DCM (50 mL), washed with 3 N aqueous HCl solution (1 × 20 mL) and brine (3 × 20 mL), and dried anhydrous Na_2SO_4, filtered, and concentrated under reduced pressure. The residue was purified by silica column chromatography (petroleum ether: EtOAc = 6:1) to give the corresponding quinazolinones **37a**, **37b**.

According to general procedure A, the demethylation of the above quinazolinones afforded the target compounds **D5**, **D12**.

*4.1.76. 5,6,7-Trihydroxy-3-isobutyl-2-(1-phenylethyl)quinazolin-4(3H)-one (**D5**)*

According to general procedure D, the product was obtained as a white solid (97 mg), yield 55%. ^{1}H NMR (400 MHz, DMSO-d_6) δ 11.75 (s, 1H), 10.30 (s, 1H), 8.83 (s, 1H), 7.36–7.20 (m, 5H), 6.61 (s, 1H), 3.80 (d, J = 15.5 Hz, 1H), 3.73 (d, J = 15.5 Hz, 1H), 4.02–3.93 (m, 1H), 3.50 (dd, J = 14.0, 7.1 Hz, 1H), 2.04 (hept, J = 6.9 Hz, 1H), 1.56 (d, J = 6.7 Hz, 3H), 0.90 (d, J = 6.7 Hz, 3H), 0.82 (d, J = 6.6 Hz, 3H). ^{13}C NMR (125 MHz, DMSO-d_6) δ 165.3, 155.1, 153.9, 146.3, 142.7, 139.9, 131.1, 128.9, 127.1, 126.9, 102.6, 100.0, 48.0, 42.3, 28.1, 22.5, 19.7, 19.6. HRMS (ESI): *m/z* calcd for $C_{20}H_{23}N_2O_4$ $[M + H]^+$: 355.1652, found 355.1655. HPLC analysis: t_R = 11.131 min, 96.2%.

*4.1.77. 2-Benzyl-5,6,7-trihydroxy-3-isobutylquinazolin-4(3H)-one (**D12**)*

According to general procedure D, the product was obtained as a white solid (95 mg), yield 56%. ^{1}H NMR (400 MHz, DMSO-d_6) δ 11.74 (s, 1H), 10.30 (s, 1H), 8.84 (s, 1H), 7.36–7.30 (m, 2H), 7.28–7.22 (m, 3H), 6.52 (s, 1H), 4.18 (s, 2H), 3.77 (d, J = 7.5 Hz, 2H), 2.08 (hept, J = 7.0 Hz, 1H), 0.86 (d, J = 6.6 Hz, 6H). ^{13}C NMR (125 MHz, DMSO-d_6) δ 165.3, 153.9, 152.6, 146.3, 140.3, 136.2, 131.0, 128.7, 128.4, 126.8, 102.3, 100.1, 49.0, 40.6, 27.8, 19.7. HRMS (ESI): *m/z* calcd for $C_{19}H_{21}N_2O_4$ $[M + H]^+$: 341.1496, found 341.1495. HPLC analysis: t_R = 11.644 min, 97.8%.

4.2. SARS-CoV-2 M^{pro} protein expression and purification

The cDNA of SARS-CoV-2 M^{pro} (GeneBank: YP_009725301.1) was synthesized and cloned into pET-28a (+) vector with codon optimization by Sangon (Sangon Biotech, Shanghai, China). The SARS-CoV-2 M^{pro} construct contains protease autoprocessing site of M^{pro} (SAVLQ↓SGFRK, arrow indicating the cleavage site) and PreScission site (SGVTFQ↓GP, arrow indicating the cleavage site) in the N terminus and C terminus, respectively. The pET-28a(+)-*SARS-CoV-2 M^{pro}* plasmid was then transformed into competent *E.coli* BL21 (DE3) cells and a single colony was picked, which was inoculated in 5 ml LB medium supplemented with 50 g/mL kanamycin and grown at 37 °C to an optical density at 600 nm of 0.8, and then induced using 0.5 mM isopropyl-β-d-thiogalactoside (IPTG). Induced cultures were grown at 25 °C for an

additional 16 h. Cells were harvested via centrifugation at 10,000 rpm for 10 min and the precipitate were resuspended in a buffer (20 mM HEPES, pH 7.5, 500 mM NaCl, 20 mM imidazole) and homogenized with an ultrahigh-pressure cell disrupter at 4 °C. The insoluble material was removed by centrifugation at 18,000 rpm for 60 min. The protein was eluted by elution buffer (20 mM HEPES, pH 7.5, 500 mM NaCl, 300 mM imidazole) after incubation with Ni-resin and washed by buffer (20 mM HEPES, pH 7.5, 500 mM NaCl, 20 mM imidazole). After auto-cleaved and cleaved by PreScission protease at 4 °C overnight, native M^{pro} was generated. In order to obtain homogeneous and pure protein suitable for crystallization and enzymatic inhibition assays, the further purification using Q column was performed with A buffer (20 mM HEPES, pH 7.5, 50 mM NaCl) and B buffer (20 mM HEPES, pH 7.5, 1 M NaCl). Protein sample was concentrated into 10 mg/mL and stored at −80 °C.

4.3. SARS-CoV-2 M^{pro} enzymatic assays

The enzyme activity of SARS-CoV-2 M^{pro} was determined using a FRET assay, which was performed as previously reported [37]. The FRET assay uses fluorogenic peptide Dabcyl-KLSAVLQSGFRKM-E-dans-NH_2 as the substrate, which was custom synthesized and obtained from GL Biochem Ltd (Shanghai, China). In brief, protease SARSCov-2 M^{pro} (600 nM at a final concentration) was mixed with compounds at the indicated concentration in 50 μL of assay buffer (20 mM Tris-HCl, pH 7.5, 10 mM EDTA, 150 mM NaCl) and incubated at room temperature for 30 min. Then, the reaction was initiated by adding 50 μL of peptide substrate to the mixture (20 μM at a final concentration) and monitored at 340 nM (excitation)/490 nM (emission) with a Tecan's Spark multimode reader. The Vmax of reactions with compounds added at the indicated concentrations compared to the solvent control was calculated and used to generate IC_{50} curves. For each compound, the half-maximal inhibitory concentration (IC_{50}) values against SARS-CoV-2 M^{pro} were measured at 10 different concentrations, and three independent experiments were performed. The data were analyzed using GraphPad Prism 8.4.3 software.

4.4. Cellular antiviral assays

A clinical isolate of SARS-CoV-2 (GenBank: MT121215.1) was propagated in Vero E6 cells and the viral titer was determined as 50% tissue culture infectious dose ($TCID_{50}$) per milliliter (mL) by CPE quantification. All the infection experiments were performed at biosafety level-3 (BLS-3) as previously reported [38]. Pre-seeded Vero E6 cells (5×10^4 cells/well) were incubated with test compounds at the indicated concentrations at 37 °C in 5% CO_2 for 1 h. Then, 100 μL of the cell supernatant was removed, followed by addition of the prepared virus-drug mixture (100 μL) to the final virus titer of 100 $TCID_{50}$/well. After infection for 1 h, the supernatant medium was discarded, and the cells were washed twice with PBS and further cultured with maintenance medium at 37 °C in 5% CO_2 for 48 h. At 48 h postinfection, the cell supernatant was collected and lysed using TRIzol LS Reagent (Invitrogen, Carlsbad, USA). Subsequently, RNA was extracted using a PureLink™ RNA Mini Kit (Thermo Fisher, Waltham, USA). The viral RNA copy number was quantified by RT-qPCR using Verso SYBR Green 1-Step qRT-PCR Kit (Thermo Fisher, Waltham, USA) on CFX96™ Real-Time PCR System (Bio-Rad, Hercules, CA) according to the manufacturer's instructions. The PCR primers targeting the N gene (nt608-706) of SARS-CoV-2 are as follows:

5′-GGGGAACTTCTCCTGCTAGAAT-3';
5′-CAGACATTTTGCTCTCAAGCTG-3'.

4.5. SARS-CoV-2 M^{pro} protein crystallization and structure determination

8 mg/mL and 12 mg/mL SARS-CoV-2 M^{pro} in buffer (20 mM Tris-HCl, pH 7.5, 10 mM EDTA, 150 mM NaCl) were incubated with 2 mM compound **D8** at 4 °C for 18 h. Then, the mixture was centrifuged at 12,500 rpm for 10 min to remove the precipitate, and the supernatant was used for crystallization. All crystallization experiments were set up at 293 K using the hanging drop approach where 1 μL of each precipitant solution was mixed with 1 μL of protein solution. Crystals were observed after a few days of incubation in 12% PEG 20,000, 0.1 M MES monohydrate (pH 6.5), which were next immersed in the crystallization solution containing 15% glycerol, and were frozen in liquid nitrogen before diffraction. The diffraction data sets were collected at the Shanghai Synchrotron Radiation Facility (SSRF, Shanghai, China) on beamline BL18U1. Using the molecular-replacement method, the structure was resolved with the Phenix program Phaser-MR [39,40], and the electron density could be clearly observed in the protein catalytic site. The eLBOW and LigandFit program in Phenix was used to fit the ligand **D8** [41]. Next, adjustment of the structural model was performed in Coot, and structure refinement in Phenix was conducted with NCS restrains [42,43]. Finally, the MolProbity program in Phenix was used to check the quality of the resulting structure [44]. Data collection and structural refinement statistics are depicted in Table S3.

Declaration of competing interest

The authors declare that they have no known competing financial interests or personal relationships that could have appeared to influence the work reported in this paper.

Data availability

Data will be made available on request.

Acknowledgements

We thank Biosafety Level 3 Laboratory, Fudan University for providing the experiment platform of cellular antiviral assay. This work was supported by grants from the National Natural Science Foundation of China (No. 82161138005, 22107117 and 22001267), China Postdoctoral Science Foundation (No. 2021M693516), and Postdoctoral Research Program of Jiangsu Province (No. 2021K218B).

Abbreviations

CCK-8	cell counting kit-8
COVID-19	Coronavirus Disease 2019
DTT	dithiothreitol
DMPK	drug metabolism and pharmacokinetics
FRET	fluorescence resonance energy transfer
HLM	human liver microsome
IPTG	isopropyl-β-d-thiogalactoside
M^{pro}	main protease
nsp	non-structural protein
PBS	phosphate buffer solution
PPB	plasma protein binding
SAR	structure activity relationship
SARS-CoV-2	severe acute respiratory syndrome coronavirus 2
TPP	triphenyl phosphite

Appendix A. Supplementary data

Supplementary data to this article can be found online at https://doi.org/10.1016/j.ejmech.2023.115487.

References

[1] WHO, WHO Coronavirus Disease (COVID-19) Dashboard. https://covid19.who.int/(accessed date: 2022.December.14).
[2] H. Ledford, Hundreds of COVID trials could provide a deluge of new drugs, Nature 603 (2022) 25–27.

[3] Y. Li, R. Tenchov, J. Smoot, C. Liu, S. Watkins, Q.A. Zhou, A comprehensive review of the global efforts on COVID-19 vaccine development, ACS Cent. Sci. 7 (2021) 512–533.

[4] M. Lipsitch, F. Krammer, G. Regev-Yochay, Y. Lustig, R.D. Balicer, SARS-CoV-2 breakthrough infections in vaccinated individuals: measurement, causes and impact, Nat. Rev. Immunol. 22 (2022) 57–65.

[5] D.R. Feikin, M.M. Higdon, L.J. Abu-Raddad, N. Andrews, R. Araos, Y. Goldberg, M. J. Groome, A. Huppert, K.L. O'Brien, P.G. Smith, A. Wilder-Smith, S. Zeger, M. Deloria Knoll, M.K. Patel, Duration of effectiveness of vaccines against SARS-CoV-2 infection and COVID-19 disease: results of a systematic review and meta-regression, Lancet (London, England) 399 (2022) 924–944.

[6] S.Y. Ren, W.B. Wang, R.D. Gao, A.M. Zhou, Omicron variant (B.1.1.529): infectivity, vaccine breakthrough, and antibody resistance, J. Chem. Inf. Model. 10 (2022) 1–11.

[7] S. Cele, L. Jackson, D.S. Khoury, K. Khan, T. Moyo-Gwete, H. Tegally, J.E. San, D. Cromer, C. Scheepers, D.G. Amoako, F. Karim, M. Bernstein, G. Lustig, D. Archary, M. Smith, Y. Ganga, Z. Jule, K. Reedoy, S.H. Hwa, J. Giandhari, J. M. Blackburn, B.I. Gosnell, S.S. Abdool Karim, W. Hanekom, A. von Gottberg, J. N. Bhiman, R.J. Lessells, M.S. Moosa, M.P. Davenport, T. de Oliveira, P.L. Moore, A. Sigal, Omicron extensively but incompletely escapes Pfizer BNT162b2 neutralization, Nature 602 (2022) 654–656.8.

[8] .

[9] R. Cannalire, C. Cerchia, A.R. Beccari, F.S. Di Leva, V. Summa, Targeting SARS-CoV-2 proteases and polymerase for COVID-19 treatment: state of the art and future opportunities, J. Med. Chem. 65 (2022) 2716–2746.

[10] K. Gao, R. Wang, J. Chen, J.J. Tepe, F. Huang, G.W. Wei, Perspectives on SARS-CoV-2 main protease inhibitors, J. Med. Chem. 64 (2021) 16922–16955.

[11] Y. Unoh, S. Uehara, K. Nakahara, H. Nobori, Y. Yamatsu, S. Yamamoto, Y. Maruyama, Y. Taoda, K. Kasamatsu, T. Suto, K. Kouki, A. Nakahashi, S. Kawashima, T. Sanaki, S. Toba, K. Uemura, T. Mizutare, S. Ando, M. Sasaki, Y. Orba, H. Sawa, A. Sato, T. Sato, T. Kato, Y. Tachibana, Discovery of S-217622, a noncovalent oral SARS-CoV-2 3CL protease inhibitor clinical candidate for treating COVID-19, J. Med. Chem. 65 (2022) 6499–6512.

[12] N. Drayman, J.K. DeMarco, K.A. Jones, S.A. Azizi, H.M. Froggatt, K. Tan, N. I. Maltseva, S. Chen, V. Nicolaescu, S. Dvorkin, K. Furlong, R.S. Kathayat, M. R. Firpo, V. Mastrodomenico, E.A. Bruce, M.M. Schmidt, R. Jedrzejczak, M. Muñoz-Alía, B. Schuster, V. Nair, K.Y. Han, A. O'Brien, A. Tomatsidou, B. Meyer, M. Vignuzzi, D. Missiakas, J.W. Botten, C.B. Brooke, H. Lee, S.C. Baker, B. C. Mounce, N.S. Heaton, W.E. Severson, K.E. Palmer, B.C. Dickinson, A. Joachimiak, G. Randall, S. Tay, Masitinib is a broad coronavirus 3CL inhibitor that blocks replication of SARS-CoV-2, Science (New York, N.Y.) 373 (2021) 931–936.

[13] D.R. Owen, C.M.N. Allerton, A.S. Anderson, L. Aschenbrenner, M. Avery, S. Berritt, B. Boras, R.D. Cardin, A. Carlo, K.J. Coffman, A. Dantonio, L. Di, H. Eng, R. Ferre, K.S. Gajiwala, S.A. Gibson, S.E. Greasley, B.L. Hurst, E.P. Kadar, A.S. Kalgutkar, J. C. Lee, J. Lee, W. Liu, S.W. Mason, S. Noell, J.J. Novak, R.S. Obach, K. Ogilvie, N. C. Patel, M. Pettersson, D.K. Rai, M.R. Reese, M.F. Sammons, J.G. Sathish, R.S. P. Singh, C.M. Steppan, A.E. Stewart, J.B. Tuttle, L. Updyke, P.R. Verhoest, L. Wei, Q. Yang, Y. Zhu, An oral SARS-CoV-2 M(pro) inhibitor clinical candidate for the treatment of COVID-19, Science (New York, N.Y.) 374 (2021) 1586–1593.

[14] R.L. Hoffman, R.S. Kania, M.A. Brothers, J.F. Davies, R.A. Ferre, K.S. Gajiwala, M. He, R.J. Hogan, K. Kozminski, L.Y. Li, J.W. Lockner, J. Lou, M.T. Marra, L. J. Mitchell Jr., B.W. Murray, J.A. Nieman, S. Noell, S.P. Planken, T. Rowe, K. Ryan, G.J. Smith 3rd, J.E. Solowiej, C.M. Steppan, B. Taggart, Discovery of Ketone-based bovalent inhibitors of coronavirus 3CL proteases for the potential therapeutic treatment of COVID-19, J. Med. Chem. 63 (2020) 12725–12747.

[15] B. Boras, R.M. Jones, B.J. Anson, D. Arenson, L. Aschenbrenner, M.A. Bakowski, N. Beutler, J. Binder, E. Chen, H. Eng, H. Hammond, J. Hammond, R.E. Haupt, R. Hoffman, E.P. Kadar, R. Kania, E. Kimoto, M.G. Kirkpatrick, L. Lanyon, E. K. Lendy, J.R. Lillis, J. Logue, S.A. Luthra, C. Ma, S.W. Mason, M.E. McGrath, S. Noell, R.S. Obach, O.B. Mn, R. O'Connor, K. Ogilvie, D. Owen, M. Pettersson, M. R. Reese, T.F. Rogers, R. Rosales, M.I. Rossulek, J.G. Sathish, N. Shirai, C. Steppan, M. Ticehurst, L.W. Updyke, S. Weston, Y. Zhu, K.M. White, A. García-Sastre, J. Wang, A.K. Chatterjee, A.D. Mesecar, M.B. Frieman, A.S. Anderson, C. Allerton, Preclinical characterization of an intravenous coronavirus 3CL protease inhibitor for the potential treatment of COVID19, Nat. Commun. 12 (2021) 6055.

[16] C. Ma, M.D. Sacco, B. Hurst, J.A. Townsend, Y. Hu, T. Szeto, X. Zhang, B. Tarbet, M.T. Marty, Y. Chen, J. Wang, G.C.- Boceprevir, 376, and calpain inhibitors II, XII inhibit SARS-CoV-2 viral replication by targeting the viral main protease, Cell Res. 30 (2020) 678–692.

[17] J. Qiao, Y.S. Li, R. Zeng, F.L. Liu, R.H. Luo, C. Huang, Y.F. Wang, J. Zhang, B. Quan, C. Shen, X. Mao, X. Liu, W. Sun, W. Yang, X. Ni, K. Wang, L. Xu, Z.L. Duan, Q. C. Zou, H.L. Zhang, W. Qu, Y.H. Long, M.H. Li, R.C. Yang, X. Liu, J. You, Y. Zhou, R. Yao, W.P. Li, J.M. Liu, P. Chen, Y. Liu, G.F. Lin, X. Yang, J. Zou, L. Li, Y. Hu, G. W. Lu, W.M. Li, Y.Q. Wei, Y.T. Zheng, J. Lei, S. Yang, SARS-CoV-2 M(pro) inhibitors with antiviral activity in a transgenic mouse model, Science (New York, N.Y.) 371 (2021) 1374–1378.

[18] W. Dai, B. Zhang, X.M. Jiang, H. Su, J. Li, Y. Zhao, X. Xie, Z. Jin, J. Peng, F. Liu, C. Li, Y. Li, F. Bai, H. Wang, X. Cheng, X. Cen, S. Hu, X. Yang, J. Wang, X. Liu, G. Xiao, H. Jiang, Z. Rao, L.K. Zhang, Y. Xu, H. Yang, H. Liu, Structure-based design of antiviral drug candidates targeting the SARS-CoV-2 main protease, Science (New York, N.Y.) 368 (2020) 1331–1335.

[19] L. Zhang, D. Lin, X. Sun, U. Curth, C. Drosten, L. Sauerhering, S. Becker, K. Rox, R. Hilgenfeld, Crystal structure of SARS-CoV-2 main protease provides a basis for design of improved α-ketoamide inhibitors, Science (New York, N.Y.) 368 (2020) 409–412.

[20] S.H. Han, C.M. Goins, T. Arya, W.J. Shin, J. Maw, A. Hooper, D.P. Sonawane, M. R. Porter, B.E. Bannister, R.D. Crouch, A.A. Lindsey, G. Lakatos, S.R. Martinez, J. Alvarado, W.S. Akers, N.S. Wang, J.U. Jung, J.D. Macdonald, S.R. Stauffer, Structure-based optimization of ML300-derived, noncovalent inhibitors targeting the severe acute respiratory syndrome coronavirus 3CL protease (SARS-CoV-2 3CL (pro)), J. Med. Chem. 65 (2022) 2880–2904.

[21] D.W. Kneller, H. Li, S. Galanie, G. Phillips, A. Labbé, K.L. Weiss, Q. Zhang, M. A. Arnould, A. Clyde, H. Ma, A. Ramanathan, C.B. Jonsson, M.S. Head, L. Coates, J. M. Louis, P.V. Bonnesen, A. Kovalevsky, Structural, electronic, and electrostatic determinants for inhibitor binding to subsites S1 and S2 in SARS-CoV-2 main protease, J. Med. Chem. 64 (2021) 17366–17383.

[22] H.X. Su, S. Yao, W.F. Zhao, M.J. Li, J. Liu, W.J. Shang, H. Xie, C.Q. Ke, H.C. Hu, M. N. Gao, K.Q. Yu, H. Liu, J.S. Shen, W. Tang, L.K. Zhang, G.F. Xiao, L. Ni, D. W. Wang, J.P. Zuo, H.L. Jiang, F. Bai, Y. Wu, Y. Ye, Y.C. Xu, Anti-SARS-CoV-2 activities in vitro of Shuanghuanglian preparations and bioactive ingredients, Acta Pharmacol. Sin. 41 (2020) 1167–1177.

[23] N. Kitamura, M.D. Sacco, C. Ma, Y. Hu, J.A. Townsend, X. Meng, F. Zhang, X. Zhang, M. Ba, T. Szeto, A. Kukuljac, M.T. Marty, D. Schultz, S. Cherry, Y. Xiang, Y. Chen, J. Wang, Expedited approach toward the rational design of noncovalent SARS-CoV-2 main protease inhibitors, J. Med. Chem. 65 (2022) 2848–2865.

[24] A. Luttens, H. Gullberg, E. Abdurakhmanov, D.D. Vo, D. Akaberi, V.O. Talibov, N. Nekhotiaeva, L. Vangeel, S. De Jonghe, D. Jochmans, J. Krambrich, A. Tas, B. Lundgren, Y. Gravenfors, A.J. Craig, Y. Atilaw, A. Sandström, L.W.K. Moodie, Å. Lundkvist, M.J. van Hemert, J. Neyts, J. Lennerstrand, J. Kihlberg, K. Sandberg, U.H. Danielson, J. Carlsson, Ultralarge virtual screening identifies SARS-CoV-2 main protease inhibitors with broad-spectrum activity against coronaviruses, J. Am. Chem. Soc. 144 (2022) 2905–2920.

[25] C.H. Zhang, E.A. Stone, M. Deshmukh, J.A. Ippolito, M.M. Ghahremanpour, J. Tirado-Rives, K.A. Spasov, S. Zhang, Y. Takeo, S.N. Kudalkar, Z. Liang, F. Isaacs, B. Lindenbach, S.J. Miller, K.S. Anderson, W.L. Jorgensen, Potent noncovalent inhibitors of the main protease of SARS-CoV-2 from molecular sculpting of the drug perampanel guided by free energy perturbation calculations, ACS Cent. Sci. 7 (2021) 467–475.

[26] H. Mukae, H. Yotsuyanagi, N. Ohmagari, Y. Doi, T. Imamura, T. Sonoyama, T. Fukuhara, G. Ichihashi, T. Sanaki, K. Baba, Y. Takeda, Y. Tsuge, T. Uehara, A randomized phase 2/3 study of Ensitrelvir, a novel oral SARS-CoV-2 3C-Like protease inhibitor, in Japanese patients with mild-to-moderate COVID-19 or asymptomatic SARS-CoV-2 infection: results of the phase 2a part, Antimicrob. Agents Chemother. 66 (2022), e0069722.

[27] C.P. Jones, K.W. Anderson, S.L. Buchwald, Sequential Cu-catalyzed amidation-base-mediated camps cyclization: a two-step synthesis of 2-aryl-4-quinolones from o-halophenones, J. Org. Chem. 72 (2007) 7968–7973.

[28] M. Hadjeri, E.L. Peiller, C. Beney, N. Deka, M.A. Lawson, C. Dumontet, A. Boumendjel, Antimitotic activity of 5-hydroxy-7-methoxy-2-phenyl-4-quinolones, J. Med. Chem. 47 (2004) 4964–4970.

[29] J. Carreras, G. Gopakumar, L. Gu, A. Gimeno, P. Linowski, J. Petuškova, W. Thiel, M. Alcarazo, Polycationic ligands in gold catalysis: synthesis and applications of extremely π-acidic catalysts, J. Am. Chem. Soc. 135 (2013) 18815–18823.

[30] X. Liu, H. Fu, Y. Jiang, Y. Zhao, A simple and efficient approach to quinazolinones under mild copper-catalyzed conditions, Angew. Chem., Int. Ed. Engl. 48 (2009) 348–351.

[31] Y. Zhang, L. Jin, H. Xiang, J. Wu, P. Wang, D. Hu, W. Xue, S. Yang, Synthesis and anticancer activities of 5,6,7-trimethoxy-N-phenyl(ethyl)-4-aminoquinazoline derivatives, Eur. J. Med. Chem. 66 (2013) 335–344.

[32] X. Tian, L. Song, E. Li, Q. Wang, W. Yu, J. Chang, Metal-free one-pot synthesis of 1,3-diazaheterocyclic compounds via I_2-mediated oxidative C–N bond formation, RSC Adv. 5 (2015) 62194–62201.

[33] S. Xue, J. McKenna, W.C. Shieh, O. Repic, A facile synthesis of C_2,N_3-disubstituted-4-quinazolone, J. Org. Chem. 69 (2004) 6474–6477.

[34] K. Liu, D. Li, W. Zheng, M. Shi, Y. Chen, M. Tang, T. Yang, M. Zhao, D. Deng, C. Zhang, J. Liu, X. Yuan, Z. Yang, L. Chen, Discovery, optimization, and evaluation of quinazolinone derivatives with novel linkers as orally efficacious phosphoinositide-3-kinase delta inhibitors for treatment of inflammatory diseases, J. Med. Chem. 64 (2021) 8951–8970.

[35] J.L. Dahlin, J.W. Nissink, J.M. Strasser, S. Francis, L. Higgins, H. Zhou, Z. Zhang, M.A. Walters, PAINS in the assay: chemical mechanisms of assay interference and promiscuous enzymatic inhibition observed during a sulfhydryl-scavenging HTS, J. Med. Chem. 58 (2015) 2091–2113.

[36] B.X. Quan, H. Shuai, A.J. Xia, Y. Hou, R. Zeng, X.L. Liu, G.F. Lin, J.X. Qiao, W.P. Li, F.L. Wang, K. Wang, R.J. Zhou, T.T. Yuen, M.X. Chen, C. Yoon, M. Wu, S.Y. Zhang, C. Huang, Y.F. Wang, W. Yang, C. Tian, W.M. Li, Y.Q. Wei, K.Y. Yuen, J.F. Chan, J. Lei, H. Chu, S. Yang, An orally available M(pro) inhibitor is effective against wild-type SARS-CoV-2 and variants including Omicron, Nat. Microbiol. 7 (2022) 716–725.

[37] W. Yu, Y. Zhao, H. Ye, N. Wu, Y. Liao, N. Chen, Z. Li, N. Wan, H. Hao, H. Yan, Y. Xiao, M. Lai, Structure-based design of a dual-targeted covalent inhibitor against papain-like and main proteases of SARS-CoV-2, J. Med. Chem. 65 (2022) 16252–16267.

[38] Y. Ni, J. Liao, Z. Qian, C. Wu, X. Zhang, J. Zhang, Y. Xie, S. Jiang, Synthesis and evaluation of enantiomers of hydroxychloroquine against SARS-CoV-2 in vitro, Bioorg. Med. Chem. 53 (2022), 116523.

[39] A.J. McCoy, R.W. Grosse-Kunstleve, P.D. Adams, M.D. Winn, L.C. Storoni, R. J. Read, Phaser crystallographic software, J. Appl. Crystallogr. 40 (2007) 658–674.

[40] P.D. Adams, P.V. Afonine, G. Bunkóczi, V.B. Chen, I.W. Davis, N. Echols, J. J. Headd, L.W. Hung, G.J. Kapral, R.W. Grosse-Kunstleve, A.J. McCoy, N. W. Moriarty, R. Oeffner, R.J. Read, D.C. Richardson, J.S. Richardson, T.

C. Terwilliger, P.H. Zwart, PHENIX: a comprehensive Python-based system for macromolecular structure solution, Acta Crystallogr. D Biol. Crystallogr. 66 (2010) 213–221.
[41] N.W. Moriarty, R.W. Grosse-Kunstleve, P.D. Adams, Electronic ligand Builder and Optimization Workbench (eLBOW): a tool for ligand coordinate and restraint generation, Acta Crystallogr. D Biol. Crystallogr. 65 (2009) 1074–1080.
[42] P.V. Afonine, R.W. Grosse-Kunstleve, N. Echols, J.J. Headd, N.W. Moriarty, M. Mustyakimov, T.C. Terwilliger, A. Urzhumtsev, P.H. Zwart, P.D. Adams, Towards automated crystallographic structure refinement with phenix, refine. Acta Crystallogr. D Biol. Crystallogr. 68 (2012) 352–367.
[43] P. Emsley, B. Lohkamp, W.G. Scott, K. Cowtan, Features and development of Coot, Acta Crystallogr. D Biol. Crystallogr. 66 (2010) 486–501.
[44] C.J. Williams, J.J. Headd, N.W. Moriarty, M.G. Prisant, L.L. Videau, L.N. Deis, V. Verma, D.A. Keedy, B.J. Hintze, V.B. Chen, S. Jain, S.M. Lewis, W. B. Arendall 3rd, J. Snoeyink, P.D. Adams, S.C. Lovell, J.S. Richardson, D. C. Richardson, MolProbity: more and better reference data for improved all-atom structure validation, Protein Sci. 27 (2018) 293–315.